THE SYNCAM FAMILY OF CELL ADHESION MOLECULES FUNCTION REDUNDANTLY TO SHAPE THE EXCITATORY SYNAPSE

by

DANIEL KEVIN FOWLER

A DISSERTATION

Presented to the Department of Biology
and the Graduate School of the University of Oregon
in partial fulfillment of the requirements
for the degree of
Doctor of Philosophy

December 2015

DISSERTATION APPROVAL PAGE

Student: Daniel Kevin Fowler

Title: The SynCAM Family of Cell Adhesion Molecules Function Redundantly to Shape the Excitatory Synapse

This dissertation has been accepted and approved in partial fulfillment of the requirements for the Doctor of Philosophy degree in the Department of Biology by:

Victoria Herman	Chairperson
Philip Washbourne	Advisor
Christopher Doe	Core Member
Judith Eisen	Core Member
Kenneth Prehoda	Institutional Representative

and

Scott L. Pratt	Dean of the Graduate School

Original approval signatures are on file with the University of Oregon Graduate School.

Degree awarded December 2015

DISSERTATION ABSTRACT

Daniel Kevin Fowler

Doctor of Philosophy

Department of Biology

December 2015

Title: The SynCAM Family of Cell Adhesion Molecules Function Redundantly to Shape the Excitatory Synapse

Functional characterization of synaptic proteins is often precluded by compensation not only among converging signaling pathways but also between structurally and functionally similar genes. One such gene family, the synaptic cell adhesion molecules (SynCAMs), contains four nearly identical members of which SynCAM1-3 are highly localized to excitatory synapses. SynCAMs have been demonstrated to have a clear synaptogenic potential when ectopically presented, either artificially or by overexpression, to developing neurons both *in vitro* and *in vivo*. Despite these observations, conflicting reports from gain- and loss-of-function experiments prevent the development of a cohesive functional model for SynCAMs in excitatory synapse formation. To overcome potential SynCAM functional redundancy and simultaneously compare effects of SynCAM knockdown and overexpression in cultured rat hippocampal neurons, I developed a tool for efficient multi-gene knockdown using artificial microRNAs. I then applied this tool with a novel analysis method which I call Mosaic Expression with Differentially Localized Reporters (MEDLR). Using MEDLR, I uncover novel synaptic phenotypes due to SynCAM1-3 knockdown which suggest

SynCAM1-3 function redundantly through postsynapse-specific mechanisms to regulate excitatory synapse number and size.

This dissertation contains both published and unpublished co-authored material.

CURRICULUM VITAE

NAME OF AUTHOR: Daniel Kevin Fowler

GRADUATE AND UNDERGRADUATE SCHOOLS ATTENDED:

University of Oregon, Eugene, OR
Colby College, Waterville, ME

DEGREES AWARDED:

Doctor of Philosophy, Biology, 2015, University of Oregon
Bachelor of Arts, Biochemistry, 2015, Colby College

AREAS OF SPECIAL INTEREST:

Neuroscience
Molecular Biology

PROFESSIONAL EXPERIENCE:

Graduate Teaching Fellow, Department of Biology, University of Oregon 2009 – 2010 and 2013 - present
Research Assistant, F.M. Kirby Neurobiology Research Center, Harvard Medical School/Children's Hospital Boston, 2007 - 2009
Research Assistant, Department of Biology, University of Alaska Anchorage, 2006 – 2007
Research Experience for Undergraduates Fellow, Department of Biology, University of Rochester, Rochester, NY, 2005

GRANTS, AWARDS, AND HONORS:

Graduate Teaching Fellowship, Department of Biology, 2013 - present
NIH Developmental Biology Training Grant, University of Oregon, 2010 - 2013
Evans B. Reid Award, Highest Departmental Honor, Department of Chemistry, Colby College, 2006
Phi Beta Kappa, Colby College, 2006
Summa Cum Laude, Colby College, 2006
Dean's Research Fund, Thesis: "Investigating the Mechanisms of a novel rRNA Quality Control System," Colby College, 2005 - 2006
Outstanding Junior Award, Department of Chemistry, Colby College, 2005

PUBLICATIONS:

Fowler, D. K., Williams, C., Gerritsen, A. T., & Washbourne, P. (2015). Improved knockdown from artificial microRNAs in an enhanced miR-155 backbone: a designer's guide to potent multi-target RNAi. *Nucleic Acids Res*, doi: 10.1093/nar/gkv1246

Hale, L. A., Fowler, D. K., & Eisen, J. S. (2011). Netrin signaling breaks the equivalence between two identified zebrafish motoneurons revealing a new role of intermediate targets. *PLoS One, 6*(10), e25841. doi: 10.1371/journal.pone.0025841

ACKNOWLEDGMENTS

I am sincerely grateful to Dr. Philip Washbourne for assistance in the preparation of this dissertation in addition to guidance on the project. Your optimism is infectious and I cannot thank you enough for all of the support and encouragement you have given me. I also thank Dr. Judith Eisen for editing the manuscript. I would also like to extend my appreciation to Dr. Scott Stewart and Dr. Kryn Stankunas for providing vectors instrumental to this investigation and for valuable discussions about cloning strategies. Lastly, I offer my thanks to everyone who has contributed to the work presented in this dissertation, with special thanks to Carly Williams and Megan Call. This work was supported in part by a Developmental Biology Training Grant from the National Institutes of Health, T32-HD07348, and a grant from the National Institutes of Neurological Disorders and Stroke, R01 NS065795, to Dr. Philip Washbourne at the University of Oregon. All animal research was conducted under IACUC protocol 13-19 at the University of Oregon.

To Alida: Thanks for waiting.

TABLE OF CONTENTS

Chapter Page

LIST OF FIGURES

CHAPTER I

INTRODUCTION

Preface: SynCAMs in Synapse Development

Correct nervous system function depends on the correct development of synapses, the points of contact and communication between neurons. Synaptogenesis, the process of synapse formation, is thought to be initiated by physical contact of adhesion molecules located on a presynaptic axon and postsynaptic dendrite of two different neurons (for review see Garner et al., 2002; Waites et al., 2005; Washbourne 2004). In addition to holding synapses together, interaction between adhesion molecules triggers the recruitment of distinct pre- and post-synaptic components. For the entirety of this dissertation I will focus on excitatory synapses, which use the neurotransmitter glutamate, and represent the vast majority of synapses in the mammalian central nervous system (CNS) (Kandel, 2013). The human cerebral cortex, which contains 80% of brain mass but only about 20% of total brain neurons (Herculano-Houzel, 2009), has been proposed to contain on the order of 10^{14} synapses (100 trillion), a figure that is nearly 1000-fold higher than the estimated number of stars in the milky-way galaxy (Drachman, 2005).

How does the brain make such a staggering number of neuronal connections, yet form them in a programmed manner which leads to a very set outcome? The process of excitatory synapse formation requires the recruitment of glutamate-filled synaptic vesicles to the presynaptic active zone as well as glutamate receptors and scaffolding molecules of the membrane-associated guanylate kinase (MAGUK) family to the postsynaptic density (PSD). A large number of adhesion molecules are known to be important for synapse formation including neurexin/neuroligins, cadherins, neuronal cell adhesion molecule (NCAM), and Ephrin-EphR (ephrin receptor) complexes (Tallafuss et al., 2010). For my dissertation, I have investigated an additional subset of synaptogenic adhesion molecules, the nectin-like synaptic cell adhesion

molecule (SynCAM) family. Despite being linked to cognitive functions and disorders as well as clearly playing a role in synapse formation, the molecular mechanisms of SynCAM-mediated synaptogenesis are ill-defined. Here, I begin with a brief review covering the current knowledge of SynCAM function in excitatory synapse development. I conclude the introduction by outlining the open questions about SynCAM function that my doctoral research intended to answer and the general approaches I used in subsequent chapters to address them.

The Nectin-like Synaptic Cell Adhesion Molecule (SynCAM) Family of Proteins

In mammals, SynCAMs are a family of 4 proteins (SynCAM1-4) belonging to the immunoglobulin superfamily of cell adhesion molecules (IgCAMs) and are encoded by the cell adhesion molecule 1-4 (CADM1-4) genes (Biederer, 2006; Thomas et al., 2008). Evolutionarily, SynCAMs are a fairly recent gene lineage since they are only found in vertebrates (Biederer, 2006), in contrast to much older synaptogenic adhesion molecules such as neuroligins, which appeared concurrently with the evolution of the first synapses around one billion years ago, or compared to even older protosynaptic adhesion molecules including neurexins and NCAM (Ryan and Grant, 2009). SynCAM1, by far the most studied family member, was identified nearly simultaneously in multiple tissue types and therefore is known by a number of different protein names including immunoglobulin subfamily member 4 (IGSF4) (Gomyo et al., 1999), spermatogenic immunoglobulin superfamily (SgIGSF) (Wakayama et al., 2001), and RA175 (Urase et al., 2001). SynCAM1 was also initially discovered as a tumor suppressor gene and termed tumor suppressor in non-small cell lung cancer (TSLC1) (Kuramochi et al., 2001). SynCAMs 3 and 4 were subsequently identified as putative tumor suppressors and were termed TSLC1-like 1 and 2 (TSLL1 and 2), respectively (Fukuhara et al., 2001). Finally, because of their similarities to nectins, another IgCAM subfamily, SynCAMs are also known as nectin-like (Necl) molecules with SynCAM1 known as Necl2, SynCAM2 as Necl3, SynCAM3 as Necl1, and

SynCAM4 as Necl4. For the entirety of this dissertation, I refer to the genes as CADMs based on their Human Genome Organization (HUGO)-defined nomenclature, and call the protein products of the CADM genes SynCAMs because they were given this name following their discovery in the context of the nervous system (Biederer et al., 2002).

Structurally, SynCAMs are a single transmembrane-spanning proteins divided into an extracellular domain containing three extracellular Ig binding domains and a small intracellular region containing two short protein interaction sequences: the FERM (F for protein 4.1, Ezrin, Radixin, Moesin) and PDZ (PSD-95, Dlg1, ZO-1) type II motifs (Biederer, 2006). The first Ig domain in the extracellular region was shown to be necessary for the *trans*-binding ability of SynCAMs (e.g. binding between pre- and postsynaptic SynCAMs) (Biederer et al., 2002). All SynCAMs have been shown to engage in homophilic *trans*-interactions (Fogel et al., 2007). Additionally, SynCAM1 and 2, SynCAM2 and 4, as well as SynCAM3 and 4 have been demonstrated to form heterophilic trans-interactions (Fogel et al., 2007). Such heterophilic binding is also known to be stronger than homophilic interactions (Fogel et al., 2007). The second and third Ig domains are known to be necessary for SynCAMs to form homo- and hetero-philic *cis*-interactions (e.g. clustering of SynCAMs in the same membrane), which potentiate their *trans*-binding ability (Fogel et al., 2011). Interestingly, the second and third Ig domains can also form cis-interactions with other transmembrane proteins, including certain receptor tyrosine kinases (RTK), as a mechanism to modulate RTK signaling (Kawano et al., 2009; Kim et al., 2011). The SynCAM intracellular tail is the most conserved region, with identical PDZ motifs (c-terminal three-amino acid YFI sequence) and nearly identical FERM motifs (Biederer, 2006) across all four mammalian protein isoforms. Both motifs have been demonstrated to bind a multitude of signaling and scaffolding molecules, and accordingly the intracellular region is an attractive candidate for signal-transducing abilities of SynCAMs (Frei and Stoeckli, 2014).

Genomic and Behavioral Associations Link SynCAMs to Cognitive Functions

A number of genetic association studies strongly link SynCAMs to the occurrence of many cognitive functions and disorders. The first such disorders were certain inherited-forms of autism spectrum disorder (ASD) (Zhiling et al., 2008). A subsequent study also linked SynCAM2 to the occurrence of ASD (Casey et al., 2012). Behavioral data in rodent models corroborated these findings because SynCAM1 knockout mice display social deficits commonly associated with autistic-like symptoms (Takayanagi et al., 2010), with aberrant accumulation of SynCAMs in endoplasmic reticulum (ER) and subsequent ER stress suggested as a cellular basis of the behavioral phenotypes (Fujita et al., 2010). Further, SynCAM1 knockout mice have impaired ultrasonic vocalization, a method for mother-offspring communication, which supports a role of SynCAMs in ASD because impaired communication is a hallmark symptom of autism (Fujita et al., 2012). More recently, SynCAMs have been strongly linked to major depressive disorders in humans. This includes being identified as markers for clinical depression (Benton et al., 2012), bipolar disorder (Redei et al., 2014), and risk of suicidality (Niculescu et al., 2015). A better understanding of SynCAM function may prove useful to the treatment of these disorders.

Considering a more general neurological function, SynCAMs are implicated in cognitive processes. For instance, behavioral data from studies of SynCAM1 knockout mice showed impairment during metrics of learning and memory (Robbins et al., 2010). A recent genomic association study has also linked altered expression of SynCAM2 to certain inherited aspects of "high-order" cognitive ability, including executive function and processing speed (Ibrahim-Verbaas et al., 2015). Remarkably, behavioral data substantiates this association because SynCAM1 knockout mice display behaviors which parallel symptoms of attention deficit hyperactivity disorder (ADHD), which is thought to arise from impaired executive functions (Sandau et al., 2012). Intriguingly, new data on synapse evolution supports a model in which SynCAMs function in high-order cognition. In such a model, the appearance and rapid

duplication of new synaptic molecules, which include SynCAMs, is thought to underlie the rapid evolution of complex neurological circuits in vertebrates due to a massive increase in synaptic proteome complexity (Ryan and Grant, 2009).

SynCAMs Are Sufficient to Induce Presynapse Formation

SynCAM1, the first SynCAM identified in the context of the nervous system, was identified by the remarkable ability to induce presynaptic protein clustering (Biederer et al., 2002). Specifically, *in vitro* experiments demonstrated that SynCAMs recruited presynaptic proteins to sites of axonal adhesion when in contact with co-cultured cells expressing SynCAM1. Furthermore, these artificially-induced contact sites formed fully functional presynaptic terminals (Biederer et al., 2002; Hoy et al., 2009; Sara et al., 2005). SynCAM2 was also demonstrated to contain the same presynaptogenic potential (Fogel et al., 2007). Further reports showed the same ability to recruit presynaptic components when artificially-synthesized SynCAMs were presented from non-biological materials such as microspheres or coated culture vessel surfaces (Breillat et al., 2007; Czondor et al., 2013). Intriguingly, this implies a presynaptic recruitment method whereby clustering of SynCAMs alone is sufficient to initiate all of the steps necessary for presynaptic formation. Later studies showed that manipulation of SynCAM levels altered the frequency of miniature excitatory postsynaptic currents (EPSCs) in pyramidal cells, both *in vitro* and *in vivo*, further implying that SynCAMs are important in active zone development (Robbins et al., 2010; Sara et al., 2005).

Mechanistically, by using overexpresssed dominant-negative forms of the proteins in cultured neurons, the ability of SynCAMs to recruit presynaptic components was shown to be mediated, at least in part, by the PDZ motif located in the intracellular region (Biederer et al., 2002; Sara et al., 2005). The FERM motif has been shown to bind and activate focal adhesion kinase (FAK) signaling in axonal growth cones, but this signaling occurred prior to axo-dendritic

contact (Stagi et al., 2010). Therefore, no clear molecular mechanism linking SynCAMs to the process of presynapse formation has yet been demonstrated.

Conflicting Results Among and Between SynCAM Gain- and Loss-of-Function Studies

Currently, the majority of data on SynCAM function stems from gain-of-function studies using overexpressed transgenic SynCAMs. For example, overexpression of SynCAM1 *in vivo* in mice increased hippocampal excitatory synapse density (Robbins et al., 2010). Results for SynCAM1 *in vitro* have been contradictory, however, because some reports show overexpression in cultured neurons increased synapse density (Cheadle and Biederer, 2012), while other reports, even from the same group, displayed no change (Burton et al., 2012; Fogel et al., 2007; Sara et al., 2005). Despite some inconsistencies, the overall data support a function of SynCAMs in endogenous synaptogenesis. Importantly, because observations suggest that SynCAMs influence synaptic density, this implies that SynCAM overexpression can initiate formation of postsynaptic, as well as presynaptic, structures. It is important to note, however, that overexpression analysis can only demonstrate that SynCAMs are sufficient for synapse formation.

Are SynCAMs necessary for synapse formation? To answer this question, loss-of-function analysis must be performed, which typically occurs through reduction of protein levels (knockdown) or genetic deletion (knockout). Currently there is a lack of such experiments for SynCAMs. One study showed that SynCAM1 knockout *in vivo* caused a small, but significant, change in both pre- and post-synaptic density in the hippocampus, suggesting that SynCAM1 was necessary for formation of both sides of the synapse (Robbins et al., 2010). Again, however, loss-of-function experiments in cultured neurons showed contradictory results because SynCAM1 knockout neurons or RNAi-mediated SynCAM1 knockdown did not show a decrease in synapse density as measured by immunostaining for synaptic components (Burton et al., 2012; Cheadle and Biederer, 2012). Therefore despite SynCAMs having a clear synaptogenic potential, the

molecular mechanisms that SynCAMs use to form synapses remain unclear, and there is a need to reconcile gain- and loss-of-function phenotypes in order to characterize synaptic functions of SynCAMs.

SynCAMs Likely Function Through Different Mechanisms Pre- and Post-Synaptically

A fundamental, but remarkable, feature of neurons is the intrinsic ability for these cells to form two polarized, functionally distinct structures: the axon and the dendrite. Within these cellular processes, each also exclusively forms pre- or post-synaptic structures, respectively. One clear reason that unique structures are formed in axons or dendrites is due to the shuttling of specific pre- or post-synaptic proteins into these already polarized parts of the cell. Accordingly most synaptic adhesion molecules are predominantly pre- or post-synaptically localized. It would be easy to assume this differentiation results in activation of structure-specific signaling complements which ultimately underlie the formation of such distinct cellular components. Therefore it has been quite surprising to find extremely similar molecular mechanisms which form pre-and post-synapses. For example, many adhesion molecules, despite being exclusively pre- or post-synaptic contain similar binding motifs and interact with the same proteins (Scheiffele, 2003; Tallafuss et al., 2010). Additionally, many of the same scaffolding molecules, predominantly from the membrane-associated guanylate kinase (MAGUK) family, are localized both pre-and post-synaptically and are heavily bound to different classes of adhesion molecules on both sides of the synapse (Dalva et al., 2007; Kim and Sheng, 2004). Finally, molecular delivery mechanisms of synaptic components, such as adapter proteins for vesicular cargo delivery, are often identical both pre- and post-synaptically (Akhmanova and Hammer, 2010; Schlager and Hoogenraad, 2009). Together, these results instead support the notion that synaptogenesis activates highly symmetrical processes on both sides of the synapse, but which end in the formation of highly specialized structures.

SynCAMs are unique in that they are among a small subset of synaptic adhesion molecules which form symmetrical, homophilic *trans*-binding interactions. Considering the notion that pre- and post-synapse formation occur through similar mechanisms coupled with the results of SynCAM overexpression which showed that SynCAMs can boost overall synapse density, it is not difficult to image that SynCAMs tap into a general mechanism both pre- and post-synaptically to initiate synapse formation. This notion immediately falls apart however, from the fact that postsynaptically-clustered SynCAMs fail to recruit any known postsynaptic component (Breillat et al., 2007; Czondor et al., 2013; Graf et al., 2004). These results show unambiguously that unlike presynapses, SynCAMs are not sufficient to form postsynapses. While this does not rule out that clustering is also necessary postsynaptically, it shows that SynCAMs require some additional factor to initiate formation of the postsynapse. It will be critical to determine the differences in signaling mechanisms for SynCAMs pre- and post-synaptically.

Project Overview: The Quest for a Cohesive Functional Model for SynCAMs

Characterizing the molecular mechanisms of SynCAM-mediated synapse formation have proven problematic. A possible reason for this difficulty is functional redundancy. In many cases characterizing molecular functions at synapses is precluded not only by massive overlap in signaling pathways and binding partners (Dalva et al., 2007; Kim and Sheng, 2004; Scheiffele, 2003), but also by functional redundancy within gene families themselves. Importantly, compensatory functions from additional family members or different adhesion molecules may hide crucial synaptic functions when manipulating individual genes. Indeed, redundancy has been observed for neurexins, neuroligins, calsyntenins, and MAGUKs, such that for each of these gene families protein reduction of at least three members is necessary to observe certain synaptic phenotypes (Gokce and Sudhof, 2013; Levy et al., 2015; Shipman et al., 2011; Um et al., 2014).

As mentioned above, SynCAMs are very structurally similar and most bind promiscuously to the same interacting molecules (Frei and Stoeckli, 2014). Combined with the observation that SynCAM1-3 have been found both pre- and post-synaptically at excitatory synapses (Fogel et al., 2007), it is likely that SynCAMs, at least to some degree, share compensatory mechanisms during synapse formation. However, SynCAM functional redundancy has never been demonstrated.

Are SynCAMs functionally redundant during synapse formation? Furthermore, do they function differently during pre- and post-synapse formation? I present in this thesis an attempt to tackle these questions. Before I could address them, however, I needed to develop novel tools. To answer the first question, a method to generate loss-of-function of multiple SynCAM family members was essential. Chapter II describes the development of an enhanced multi-gene knockdown method, which I applied for the efficient, simultaneous depletion of multiple SynCAM isoforms in a cultured rat hippocampal neuron system. To answer the second question, I required a very robust, controlled assay to allow separation of pre- and post-synaptic effects. Chapter III describes the generation of a novel culture-based assay which allows discrimination of pre- and post-synaptic effects following the application of the knockdown tools presented in Chapter II. Chapter III further explores the effect of SynCAM1-3 knockdown in this novel assay to determine if SynCAMs function redundantly, and if they differentially mediate pre- and post-synapse development.

This dissertation includes previously published and unpublished co-authored material. Chapter II contains material that was previously published in *Nucleic Acids Research* in 2015 with co-authors Carly Williams, Alida T. Gerritsen, and Philip Washbourne. Chapter III contains unpublished co-authored material with co-authors Carly Williams, Scott Stewart, Kryn Stankunas, and Philip Washbourne.

CHAPTER II

IMPROVED KNOCKDOWN FROM ARTIFICIAL MICRORNAS IN AN ENHANCED MIR-155 BACKBONE: A DESIGNER'S GUIDE TO POTENT MULTI-TARGET RNAI

This work was previously published in Nucleic Acids Research (doi:10.1093/nar/gkv1246) in November, 2015. The work described in this chapter was co-authored by myself, Carly Williams, Alida T. Gerritsen, and Philip Washbourne. Carly Williams helped run many of the experiments. Alida T. Gerritsen performed bioinformatic comparisons presented in Figure 2. Philip Washbourne contributed to the experimental design and helped edit the manuscript. I conceived the study and experimental design, ran the majority of the experiments, analyzed the data, and wrote the paper.

INTRODUCTION

The advent of molecular techniques based on RNA interference (RNAi) has opened many avenues to researchers for genetic manipulation (reviewed in ref. 1). RNAi is a cellular pathway which uses short interfering RNAs (siRNAs) for posttranscriptional gene regulation mainly through the biogenesis and use of microRNAs (miRNAs) (for review see refs. 2-4). Endogenous miRNAs are hairpin-like secondary structures found in many primary RNA transcripts (pri-miRNAs). In the nucleus, the microprocessor Drosha/DGCR8 complex binds and cleaves the basal stem of pri-miRNAs to liberate the stem-loop precursor miRNA (pre-miRNA). Pre-miRNAs are then exported from the nucleus where the loop is cleaved by Dicer/TRBP to form a mature RNA duplex. The guide strand, also known as targeting strand, is separated from the passenger strand and loaded onto an argonaute protein in the RNA induced silencing complex

(RISC), which then targets complementary mRNA transcripts for degradation or translational repression.

Common methods for RNAi involve the use of vector-based expression of ~19-24 nucleotide short hairpin RNAs (shRNAs) or synthetic targeting sequences embedded in endogenous miRNA backbones (artificial miRNAs, amiRNAs). Although functional backbones for amiRNA expression have been made from a number of naturally-occurring miRNAs (5-10), the two most commonly used amiRNA scaffolds are derived from either miR-30 or the synthetic inhibitory BIC/miR-155 RNA (SIBR) (11,12), especially since commercial vectors have been developed using these backbones (Open Biosystems Expression Arrest™, GE Dharmacon and Block-iT Pol II miR RNAi™, Life Technologies, respectively). amiRNAs are embedded in sequences driven by RNA Polymerase II (Pol II) promoters, whereas shRNA expression is typically driven by constitutive Pol III promoters, such as H1 or U6. While there are conflicting reports, shRNAs generally outperform miRNAs for knockdown efficacy, likely due to higher shRNA expression levels using Pol III promoters (13-16).

Potent knockdown using shRNAs often comes at a cost, however, as at least three problems frequently arise from shRNA overexpression. First, high levels of shRNAs can cause toxicity due to oversaturation of the endogenous miRNA pathway (17-19). Oversaturation may even result in lethality during *in vivo* studies (20). amiRNAs are typically expressed at much lower levels and do not saturate endogenous RNAi pathways (13,21,22). As such, amiRNAs are suitable for studies where shRNAs were toxic (23-25). Second, shRNA sequences are usually designed with perfectly-matched guide and passenger strands. In contrast, amiRNAs are often designed with central mismatches between the guide and passenger strands, which may reduce off-target effects by decreasing unwanted passenger strand incorporation into RISC (26,27). Third, shRNAs often induce an immune response which may compound or mask RNAi-specific

effects (28-33). Use of amiRNAs may circumvent this problem by avoiding immune activation (23,34).

amiRNAs allow greater vector design flexibility and diversity of application compared to shRNAs. For example, amiRNAs can be co-expressed with transgenes from a single cistron driven by Poll II promoters, such as cell-specific or conditional promoters (16,24,35-37). amiRNAs can also be placed in an intron so that miRNA processing does not interfere with transgene expression (11,38). Indeed, it was originally shown that intronic SIBR amiRNAs are more potent than their exonic counterparts (11). Further, amiRNAs can easily be chained in tandem, either to increase knockdown efficiency or to target multiple genes, without the need of dedicated promoters for each hairpin sequence (9,11,39,40). Chained amiRNAs are particularly powerful tools for systems requiring multiple-target knockdown, such as studying functionally-redundant genes. For example, functional compensation often arises from gene duplications, which can mask phenotypes in single-knockout animals (41). Targeted knockdown of multiple genes can be used to overcome functional redundancy, without the need for more difficult and laborious techniques such as conditional multi-gene knockout animals. Furthermore, combinatorial amiRNA holds great promise for many gene therapies including those targeting rapidly-evolving pathogens (42,43) or human diseases caused by multiple factors, including cancer (44,45)

Currently, many researchers choose to use shRNAs based solely on the potential for greater knockdown. Because of the advantages afforded by miRNAs, enhanced knockdown rivalling that of shRNAs would be quite beneficial for many applications. Targeted optimization of miRNA scaffolds using insights gained from an improved understanding of miRNA function holds promise for increasing knockdown potency (26,46). For example, a recent deep-sequencing study uncovered conserved sequence elements of miRNA backbones that are associated with increased miRNA biogenesis and enhanced knockdown efficiency, including common UG and

CNNC motifs at the basal stem region (47). Using this knowledge, an improved amiRNA backbone that enhanced microprocessor cleavage and knockdown potency, termed "miR-E", was created by reintroduction of the wild-type CNNC motif into the commonly used miR-30 scaffold (46).

Despite enormous advancement in algorithms and rules for designing functional RNAi sequences over the last decade, the process of screening for potent sequences is often time-consuming, costly and laborious. In the present study, we suggest important criteria for effective amiRNA design. We also create and systematically test an enhanced SIBR (eSIBR) backbone containing exogenous UG and CNNC motifs at the basal stem which boosts relative amiRNA knockdown potency compared to the wild-type SIBR (wtSIBR) backbone. We find chaining amiRNAs targeting different genes is itself sufficient to enhance knockdown of each individual gene, and that eSIBR outperforms wtSIBR for multi-gene knockdown in lentiviral-transduced primary cultured hippocampal neurons. Taken together, this study presents a template for developing and expressing amiRNAs for potent multi-target RNAi.

MATERIAL AND METHODS

Expression vectors and constructs

GFP-SIBR vectors. EGFP coding sequence was inserted into HindIII and BamHI sites of pcDNA3 (Invitrogen) to make CMV-GFP. The 150 nucleotide SIBR minimal region was amplified from Ui4-SIBR-GFP (11) and inserted between the EcoRI and XbaI sites of CMV-GFP to make CMV-GFP-SIBR using primers SIBR_f and SIBR_r. Ui4-SIBR-GFP was graciously provided by Dr. David Turner (University of Michigan). To allow cloning of miRNA targeting sequences into the SIBR cassette using BbsI as previously described (11), the single native BbsI site in CMV-GFP-SIBR was silently mutated by site-directed mutagenesis (Agilent). Site-directed mutagenesis was used to introduce basal UG and CNNC motifs and to generate GFP-

eSIBR (Figure 3A). The G at position -15 and +14 were also changed to U in order to maintain the proper predicted folded structure. The CNNC motif was inserted beginning at position +19 due to an unusual 2 nucleotide bulge at positons +2 and +3 in the predicted folded miR-155 backbone. The inserted position of the CNNC motif is therefore equivalent to the +17 position of miRNAs without a 3' mismatch bulge. To complete the CNNC motif, the C at position +18 was changed to U because it was shown that a C preceding the CNNC motif of miR-30 inhibited knockdown efficiency (46). The GFP-eSIBR vector has been deposited with Addgene (www.addgene.org). amiRNA sequences (Supplementary Table S1) were cloned into the SIBR cassette and chained as previously described (11). Scrambled control guide strand sequences used were scrambled1: 5'-AUUCUAAUACUACGUUCCGCAU-3', scrambled2: 5'-ACAACUUGUAUAUCGCGCAACU-3' and scrambled3: 5'-GAUCUUAUACUCGUGAUUGAGA-3'.

Viral Vectors. The gateway cloning system (Invitrogen) was used to make viral vectors. To express miRNAs intronically, entry vector pME-SIBR was cloned by amplification of UI4-SIBR-GFP immediately following the Ubiquitin C promoter and ending shortly after the final intron/exon boundary using primers Ui4_SIBR_attBf and Ui4_SIBR_attBf , then inserted into pDONR221. The pME-SIBR vector has been deposited with Addgene. Single or triplet SIBR cassettes were shuttled to pME-SIBR from GFP-SIBR using EcoRI and XhoI. For entry vector p5E-CMV the CMV promoter sequence of pcDNA3 was cloned into pDONR221 P4-P1R using primers CMV_attBf and CMV_attBr. For entry vector p3E-nlsGFP, nlsGFP was amplified from pME-nlsGFP (48) and inserted into pDONR221 P2R-P3 with primers nlsGFP_attBf and nlsGFP_attBr. The viral vector LV-CMV-SIBR-nlsGFP was made using the above entry vectors in an LR reaction with a Gateway-compatible third generation lentiviral destination vector kindly provided by Dr. Kryn Stankunas (University of Oregon).

HA-Reporter vectors. Generation of HA-Cadm1 and HA-Neuroligin1 vectors were previously described (49,50). To make HA-Cadm2 and HA-Cadm3 expression vectors, Cadm2 and Cadm3 coding regions were amplified by PCR from mouse cDNA and inserted into pcDNA3 using primer pairs Cadm2_f/r for Cadm2 and Cadm3_f/r for Cadm3. HA tags were then inserted following the signal sequences with the megaprimer PCR technique using megaprimer HA-Cadm2_mp for Cadm2 and HA-Cadm3_mp for Cadm3. HA-Neuroligin2, HA-Neuroligin3, HA-Neurexin1, HA-Neurexin2, and HA-Neurexin3 vectors were kindly provided by Dr. Peter Scheiffele (University of Basel, Switzerland) and have been previously described (51-53). All primer sequences are listed in Supplementary Table S2

amiRNA design

amiRNA sequences were designed with considerations of previously described criteria for effective shRNA and miRNA sequences where possible (54-58). Briefly, specific nucleotides included a U or A (preference for U) at guide position 1 relative to the 5' microprocessor cleavage site, U/A preferences in positions 2-7, 10-14, and 17, and G/C preferences in positions 19-21. Another prominent consideration was to design sequences with an optimal G/C content between 36.4 to 45.5% when possible. Guide strands were also designed to be 2 nucleotides longer than the passenger strand as in the original report (11). Mismatches were positioned when possible to make three general structural categories: 1.) a "loop" mismatch where 3-5 adjacent nucleotides of the guide strand were not base paired to the target strand, 2.) a "3bp-spaced" mismatch where 2 single guide strand nucleotide mismatches were separated by 3 guide/passenger base pairs and 3.) a "4bp-spaced" mismatch where 2 single guide strand nucleotide mismatches were separated by 4 guide/passenger base pairs. Of our 129 amiRNA sequences, 9 did not fold into a secondary structure fitting the above categories and 6 amiRNA sequences were designed with two alternative mismatch structures (Supplementary Table S1).

For all amiRNA sequences, mismatches ranged between guide positions 11 and 17. Predicted RNA secondary structures were generated using Mfold (59). Schematics of miRNA secondary structures were drawn using VARNA (60).

Mismatch structure and sequence-specific biases

We determined the frequency (with a range of 0 to 1) of mismatch structures within our effective, ineffective, and total amiRNA sequences. For each structural class, we calculated effective and ineffective amiRNA structure bias as the deviation of the observed frequency from the expected frequency of the total amiRNA set. Frequencies of nucleotides at specific guide strand positions were determined for our empirically-screened inefficient amiRNA sequences, and the combined efficient amiRNA set containing our screened efficient sequences and additional sequences obtained from primary literature (Supplementary Table S1). Nucleotide frequencies were calculated using custom scripts built using the ShortRead package (61) in R (R Foundation for Statistical Computing, Vienna, Austria). Nucleotide frequency biases were calculated as deviation of the observed nucleotide frequency at each position of the guide strand from an unbiased expectation of 0.25. To remove the effect of design bias, we normalized the frequency bias of the effective amiRNAs by subtracting frequency biases for the ineffective amiRNAs.

qRT-PCR

First-strand cDNAs were synthesized from total RNA isolated following COS7 cell transfections using Superscript III reverse transcriptase (Invitrogen). For experiments comparing pri-miRNA levels of target sequences in different SIBR backbones, cDNAs were created using oligodT primers for 50 minutes at 50°C. For experiments comparing chaining-based effects, random hexamer primers were used with synthesis at 55°C for 1 hour. In both cases, pri-miRNA levels were first normalized to gapdh levels as a loading control. Rat gapdh primers were

qRat_gapdh_f/r. For experiments comparing pri-miRNA levels of target sequences in different SIBR backbones the primer pair qSIBR_f/r flanking the 5' and 3' microprocessor cut sites in the SIBR backbones was used. For experiments comparing chaining-based effects, primer qSIBR_f was used with hairpin–specific reverse primers for cadm1.1358 (qCadm1.1358_r) and nlgn2.1283 (qNlgn2.1283_r). qRT-PCR was performed using SYBR Green reagents (Kapa Biosystems) on a StepOnePlus Real-Time PCR System (Applied Biosystems). Values and relative expression levels were compared using the $\Delta\Delta C_t$ method. Primer sequences are listed in Supplementary Table S2.

Lentiviral production and titration

$2.5x10^6$ HEK293T cells were plated per 10-cm tissue culture dishes in 10ml of DMEM (Invitrogen), 10%FCS, 25 units/ml penicillin & 25 µg/ml streptomycin (Sigma). ~24 h after plating, cells were transiently transfected using calcium-phosphate with 20 µg LV-CMV-SIBR-nlsGFP vectors and packaging vectors (10 µg pMDL g/p RRE, 5 µg pRSV-Rev, 6 µg pVSV-G) (62). 6-8 h later media was replaced with 6ml/plate of fresh medium. Medium was collected 48-72 h after transfection and centrifuged at 3000xg for 5 min at RT. Supernatant was passed through a 0.45 µm syringe filter and virus was concentrated by centrifugation on a 150,000 MWCO column (Pierce). 20,000 HEK293T cells were plated per well of a 12-well plate and transduced with serial dilutions of concentrated lentivirus. 4-5 days after transduction, titres were calculated by flow cytometry on an Attune® acoustic focusing cytometer (Applied Biosystems) for GFP+ cells. Infectious lentiviral particles/µl were calculated from viral dilutions where cells were transduced in the linear range (5-20% GFP+ cells).

COS7 cell culture and transfection

COS7 cells (ATCC® Manassas, VA) were plated at a density of 50.000 cells per well of a 12-well tissue culture plate and maintained in DMEM (Invitrogen), 10%FCS, 25 units/ml penicillin & 25 μg/ml streptomycin (Sigma). ~24 h after plating, media was replaced with DMEM, 10% FCS without pen/strep and cells were transiently transfected with lipofectamine 2000 (Invitrogen) for ~18 h, at which point media was replaced with DMEM, 10% FCS with pen/strep. 1 μg of reporter vector and 2 μg of GFP-SIBR vectors per well were co-transfected for knockdown experiments. For transfections for harvesting total RNA for qPCR, 1 μg of GFP-SIBR vectors were transfected per well. Cells were harvested 48-72 h following transfection.

Primary hippocampal cell culture and viral transduction

Hippocampal cultures were prepared from embryonic day 19 Sprague-Dawley rat pups as described (63), with minimal modifications. 100,000 cells were plated per well of a 12-well tissue culture plate coated with poly-L-lysine (Sigma, St. Luis, MO) in plating media (MEM (Invitrogen), 10% FCS, 20 mM dextrose, 25 units/ml penicillin and 25 μg/ml streptomycin) and incubated for 5-6 h. Media was then changed to maintenance media (Neurobasal medium (Invitrogen), 1X B-27 supplement (Invitrogen), 0.5 mM Glutamax (Invitrogen), 50 units/ml penicillin, 50 μg/ml streptomycin, and 0.07% β-mercaptoethanol). Half changes of maintenance media were performed every 3-4 days in culture. 200,000 infectious viral particles were added per well to transduce neurons at 2DIV. Cells were harvested at 14DIV. Studies were conducted in accordance with University of Oregon Institutional Animal Care and Use Committee protocols and in compliance with NIH guidelines for the care and use of vertebrate animals.

Quantitative western blotting

Cells were harvested after a brief wash with 1X PBS using 2X Laemmli buffer (125 mM Tris pH 6.8, 20% glycerol, 4% SDS, 0.004% bromophenol blue) with 5% beta-mercaptoethanol. Samples were heated at 95°C for 5 minutes, and proteins were separated by SDS-PAGE before transfer to a nitrocellulose membrane. Membranes were blocked for 1h with 3% milk in PBS and treated with primary antibodies in 3% milk/PBS overnight at 4°C. The next day membranes were washed 3 x 5 min with PBS, shaken with secondary antibody in 3% milk/PBS for 1 hr at RT, washed 3 x 5 min with PBS and imaged with an Odyssey-Fc quantitative western blot system (LI-COR). Intensities were quantified per manufacturer's instructions. Primary antibodies used were actin (mouse, 1:2000, Millipore), HA.11 (mouse, 1:2000, Covance), GFP (chicken, 1:2000, Aves Labs), Cadm1 (chicken, 1:1000, MBL International), Cadm3 (rabbit, 1:1000, Sino Biological), and Pleio-Cadm (rabbit, 1:1000, Pierce). Secondary antibodies used were anti-mouse and anti-chicken IRDye 680RD, anti-rabbit and anti-chicken IRDye 800CW (donkey, 1:1000, LI-COR). Intensities were normalized to actin loading controls. Knockdown efficiency was calculated by setting levels relative to the empty GFP-wtSIBR controls for COS7 cell experiments or uninfected (no virus) controls for neuronal cultures. Potency-of-knockdown was a metric with arbitrary units used to compare relative changes in knockdown efficacy between two conditions, and was calculated by dividing remaining reporter level (100% - knockdown efficiency) in a control condition (such as amiRNA in wtSIBR backbone or single amiRNA cassette) by the remaining reporter level in a comparison condition. Potency-of-knockdown for the control condition was set to 1.

Statistical analysis

Where noted, p values obtained by statistical comparisons of two sample groups used Student's two-tailed, unpaired t-tests and comparisons of more than two sample groups used one-way

ANOVAs followed by Tukey's post-hoc pairwise comparisons. For mismatch structure analysis, we performed Pearson's χ^2-tests (α=0.05) which compared observed versus expected number of effective amiRNA and ineffective amiRNAs for each mismatch class. Expected effective and ineffective amiRNA numbers for each mismatch group were calculated using frequencies of the total amiRNA set. For nucleotide frequency analysis at specific guide strand positions, we performed individual Pearson's χ^2-tests for actual counts (α=0.01) or normalized expectations (α=0.001) which compared A,U,G and C numbers at each guide strand position against an unbiased expectation of equal base frequencies. p values were adjusted using Šidák correction for inflated α levels due to multiple comparisons. χ^2-tests and t-tests were conducted in Microsoft Excel. ANOVAs, Tukey's post-hoc analysis, and Šidák corrections were performed in R.

RESULTS

Screening empirically-designed amiRNAs uncovers sequence-specific and structural features associated with efficient sequences

To screen for effective amiRNA sequences, we used a vector with the Pol II cytomegalovirus (CMV) promoter driving expression of EGFP with the original 150bp wtSIBR cassette (11) in an exon immediately following the EGFP stop codon (GFP-wtSIBR, Figure1A and 1B). We tested a set of 22-nucleotide long amiRNA targeting sequences (total of 129, Supplementary Table S1) by inserting into the guide strand position of the wtSIBR backbone (Figure 1A). amiRNAs targeted a total of nine genes spanning three neuronal cell adhesion protein families. Targeted genes were cadm1-3, nlgn1-3 and nrxn1-3 which code for the proteins Cell adhesion molecule (Cadm) 1-3, Neuroligin1-3 and Neurexin1-3, respectively. As reporters for each targeted gene, we used Pol II-promoted hemagglutinin epitope-tagged constructs (HA-reporter). Using quantitative western blotting, we screened for effective amiRNA sequences co-transfecting amiRNA-expressing vectors with their counterpart HA-reporter vectors in COS7

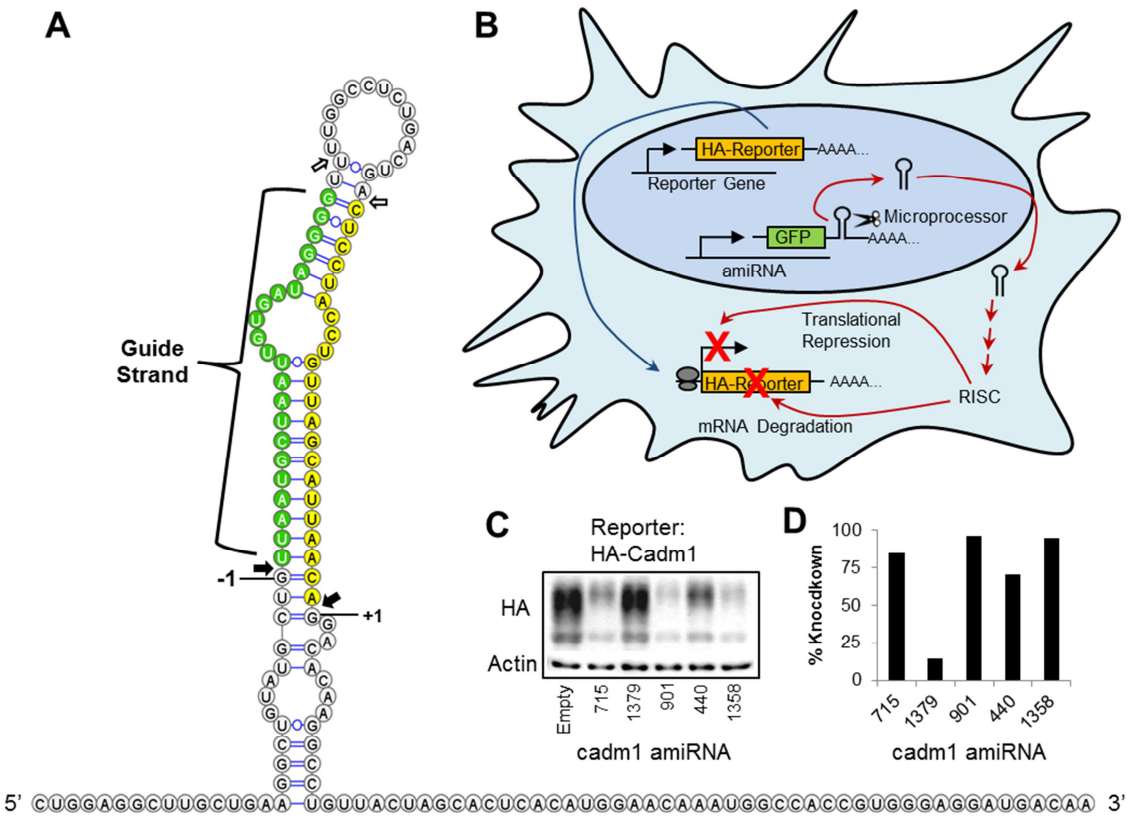

Figure 1. Overview of the wtSIBR cassette and amiRNA screening. (**A**) Nucleotide sequence of the 150-bp wtSIBR cassette from mouse and predicted miRNA secondary structure. The guide and passenger strands are labelled green and yellow, respectively. Microprocessor cleavage sites are marked with closed arrows and the +1 and -1 nucleotides relative to cleavage are indicated. Dicer cleavage sites are marked with open arrows. (**B**) Schematic representation of amiRNA screening. COS7 cells were co-transfected with an HA-tagged reporter construct and an amiRNA cloned into the guide strand position of the wtSIBR backbone located in an exon following the GFP open reading frame (GFP-SIBR). amiRNAs are liberated by the microprocessor, exported from the nucleus where they are further processed and loaded into the RNA-induced silencing complex (RISC). Effective sequences lead to reduced reporter levels due to mRNA degradation or translational repression. (**C**) Representative quantitative western blot using an HA antibody to measure reporter expression and (**D**) calculated reporter knockdown efficiency of cadm1 amiRNAs. Knockdown percentage was calculated relative to reporter co-transfection with a vector containing an empty wtSIBR cassette (empty). Actin was used as a loading control.

cells (Figure 1B). Cultures co-transfected with efficient amiRNA sequences showed decreased reporter expression compared to control cultures co-transfected with a GFP-wtSIBR vector lacking an amiRNA targeting sequence (empty) (Fig. 1C,D). Sequences which resulted in >25% reporter knockdown were considered effective and all others were considered ineffective. 50

amiRNAs were effective and 79 were ineffective for reporter knockdown (Supplementary Table S1).

Because SIBR-based amiRNAs are frequently designed with guide/passenger strand mismatches (11), we wanted to determine if mismatch structure was associated with knockdown efficiency. We grouped amiRNAs into three general categories that mimicked predicted naturally-occurring miR-155 secondary structures (Figure 2A). We found that effective hairpins were less likely to contain a loop mismatch whereas ineffective hairpins were more likely to contain a loop mismatch (Figure 2B). We also noted that effective hairpins tended to contain the 3bp-spaced mismatch structure ($p=0.07$, Pearson's χ^2-test) and had little bias for or against the 4bp-spaced mismatch structure. The observed tendency for successful amiRNAs to contain the human mismatch structure may indicate a species-specific preference, because COS7 cells are a primate-derived line (African green monkey). Furthermore, G/C content of effective versus ineffective amiRNA sequences were compared and we found the G/C content of effective hairpins to be significantly less than ineffective hairpins (effective = 40.1% G/C, ineffective = 43.5% G/C) (Figure 2C).

Next, we examined the primary sequence factors that influenced knockdown efficiency. To do so, we mined primary literature to obtain an additional 133 effective SIBR amiRNA sequences to increase our comparison power. We then calculated the nucleotide frequency bias at individual guide strand positions for the combined effective amiRNA set (n = 183) and our

---

Figure 2 (next page). Distinct structural features are associated with effective and ineffective amiRNA sequences. (**A**) Example miR-155 nucleotide sequences from different organisms and predicted secondary structures of distinct guide/passenger strand mismatches. (**B**) Frequency bias of different mismatch structures found in effective and ineffective amiRNA sequences. Effective amiRNA n=50, ineffective amiRNA n=84, **p<0.01, Pearson's χ^2-test. (**C**) G/C nucleotide content of effective and ineffective amiRNA sequences. Effective amiRNA n = 50, ineffective amiRNA n=79, ***p<0.001 Student's two-tailed t-test. Error bars represent s.e.m. (**D**) Nucleotide frequency bias of effective and ineffective amiRNA sequences and (**E**) Normalized U/A or G/C nucleotide frequency bias of effective amiRNA sequences. Nucleotide positions are relative to the 5' microprocessor cleavage site. Effective amiRNA n =183, ineffective amiRNA n = 79, **p<0.01, ***p<0.001 Pearson's χ^2-test with Šidák correction for multiple comparisons.

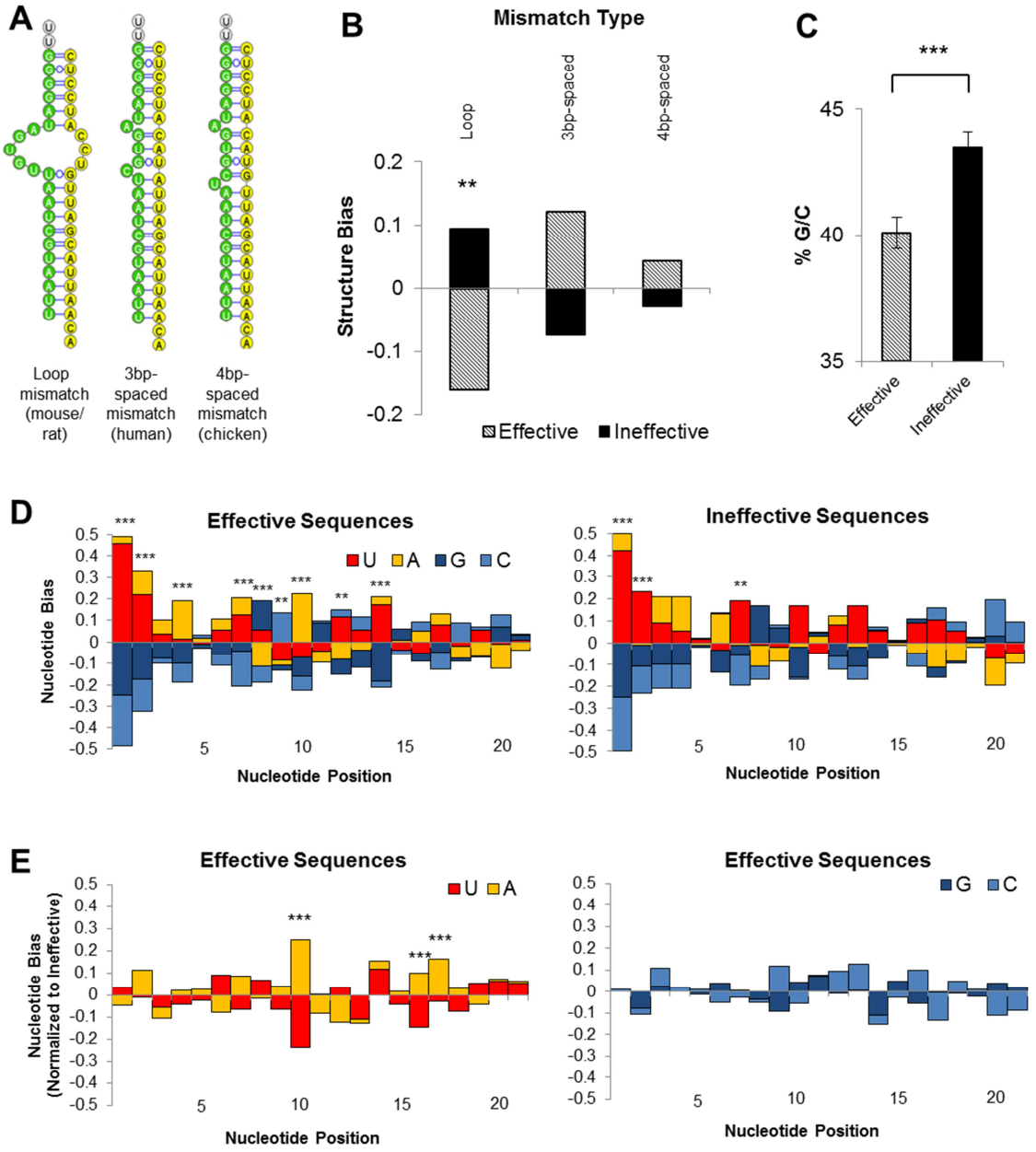

ineffective amiRNAs (n = 79) (Figure 2D). Note that we did not compare position 22 because many of the hairpins we obtained from the literature were cloned into a specific miR-155 backbone (pcDNA^{TM}6.2-GW/EmGFP-miR) where position 22 is always a G. As most amiRNAs are designed using common algorithms and guidelines, it was not surprising to find significant enrichments (α=0.01) of either U, A, or both at position 1, 2, 4, 7, 10, 12, and 14 in effective amiRNA sequences. We did note unexpected enrichment of G at position 8 and C at position 9.

Also as expected, both the effective and ineffective sequences displayed a G/C content asymmetry, with A/U-rich 5' and G/C-rich 3' ends. This asymmetry has been shown to influence guide strand selection, is strongly associated with effective target sequences, and is a major criterion for effective siRNA design (64,65). Additionally, nucleotide frequencies at specific positions were quite similar in effective and ineffective sequences, likely indicating design bias for both sets. To eliminate design bias, we normalized the effective sequence nucleotide frequency by subtracting the values of the ineffective dataset. Because our ineffective amiRNA set was smaller than the combined effective amiRNA set, we made our analysis more stringent (α=0.001). Normalization removed all of the enrichments noted above except for position 10, where, strikingly, effective amiRNA sequences were likely to contain an A but not a U (Figure 2E). We did note a significant, but smaller, enrichment of A and depletion of U at positions 16 and 17. We did not find any significant bias for G or C at any position (Figure 2E). Taken together, these results highlight important criteria for designing effective amiRNA sequences.

Introduction of UG and CNNC motifs creates an enhanced SIBR (eSIBR) backbone

Because recent studies have shown that targeted adjustments to the miR-30 backbone can increase knockdown efficiency (26,46), we tested whether modifications to the wtSIBR backbone could also increase amiRNA knockdown potency. Auyeung and colleagues established that two key sequences at the basal stem in human miRNAs, the UG motif at positions -14 and -13 relative to the 5' microprocessor cleavage site and the CNNC motif beginning between positions +16 and +18 relative to the 3' microprocessor cleavage site, are associated with efficient miRNA processing and target knockdown (47). Neither of these motifs are present in the wtSIBR backbone, so we introduced the motifs singly or in combination to GFP-wtSIBR to create modified GFP-SIBR scaffolds (Figure 3A).

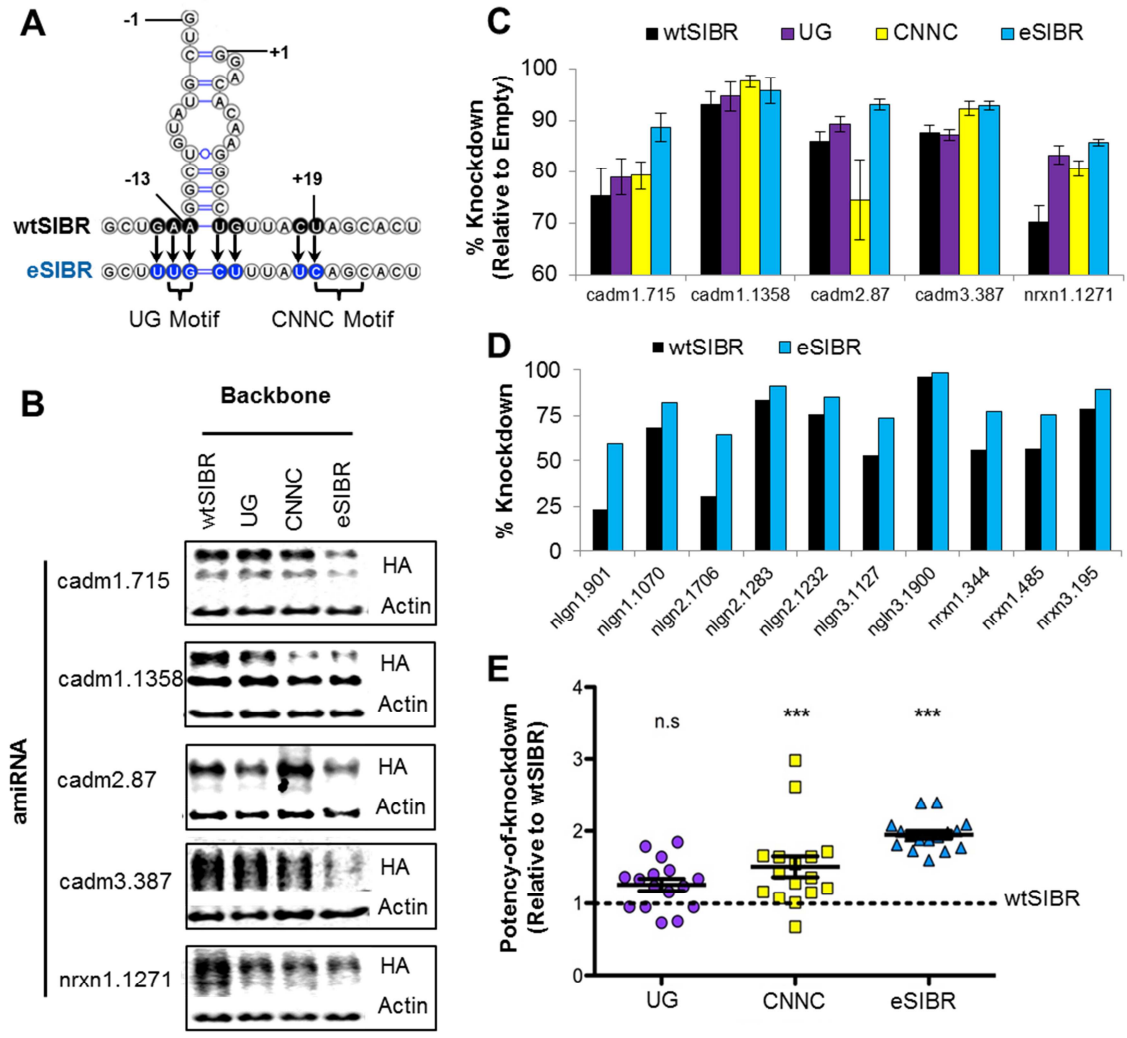

Figure 3. The eSIBR backbone enhances knockdown potency. (**A**) Nucleotide substitutions on and near the miR-155 basal stem which added the indicated UG and CNNC motifs to create the eSIBR backbone. Black circles indicate the wild-type sequence; blue circles are the modified sequence. Nucleotide numbers are relative to microprocessor cleavage sites. (**B**) Representative western blots and (**C**) quantification of reporter knockdown efficiency from data in Supplementary Figure S1 (see the Appendix) in COS7 cells co-transfected with the indicated amiRNAs in wild-type or modified SIBR backbones. Knockdown percentage was calculated relative to reporter co-transfections with a control vector containing an empty wtSIBR cassette (empty, not shown). Actin was used as a loading control. cadm1.715 and nrxn1.1271 n = 4 independent experiments, all others n = 3 independent experiments. (**D**) Reporter knockdown efficiency as in (C) from single experiments with additional amiRNAs in the wtSIBR or eSIBR backbone. (**E**) Comparison of potency-of-knockdown between constructs containing amiRNAs in modified backbones (plotted points) relative to their counterparts in the wtSIBR backbone (dotted line). If more than one experiment was conducted for an amiRNA, the average value is plotted. n = 16 amiRNAs, ***p<0.001, n.s. = not significant, one-way ANOVA with Tukey's post-hoc comparison to the wtSIBR backbone group. For all graphs error bars represent s.e.m

We evaluated the effect of modified SIBR backbones on amiRNA knockdown efficiency for 16 of our effective amiRNA sequences (Figure 3B-D and Supplementary Figure S1; see the Appendix for supplementary figures). The majority of these amiRNA sequences induced robust knockdown when expressed from the wtSIBR backbone (Figure 3C and 3D). In order to be confident that our quantitative Western blot assay was suitable to measure further knockdown enhancement, we tested the precision of the assay for measuring small differences in protein levels. We found that our assay was able to reliably and accurately measure differences as low as 10% of HA-reporter protein levels (Supplementary Figure S2). These results demonstrate that our quantitative Western blot assay is well suited to monitor differences in knockdown efficiencies due to backbone modifications.

We performed 3-4 replicate experiments comparing knockdown efficiencies for five of our potent (>70% knockdown) amiRNA sequences expressed from the wtSIBR or modified backbones (Figure 3B and 3C, Supplementary Figure S1). Changes in knockdown efficacy in response to introduction of single UG or CNNC motifs varied considerably for individual amiRNA sequences (Figure 3C). In contrast, introduction of both UG and CNNC motifs into the SIBR backbone enhanced reporter knockdown for all 16 amiRNA sequences tested (Figure 3C and 3D). We named this backbone containing both motifs the enhanced SIBR (eSIBR) scaffold. Because the range of reporter knockdown from amiRNAs in the wtSIBR backbone was large (~25% to >90%, Figure 3C and 3D) and were difficult to compare directly, we used a relative metric that is independent of absolute knockdown percentage. This metric, which we call potency-of-knockdown, is the inverse of the amount of the remaining reporter level compared to a control condition; an amiRNA that reduced the remaining protein to 1/2 of the control amount had a 2-fold potency-of-knockdown, one that reduced remaining reporter to 1/3 had a 3-fold potency of knockdown.. We used this metric to compare knockdown efficacy of amiRNA sequences in modified backbones relative to corresponding wtSIBR amiRNAs. The eSIBR

backbone reproducibly boosted potency-of-knockdown an average of ~2-fold over counterpart sequences in the wtSIBR backbone (Figure 3E).

The eSIBR backbone enhances cleavage by the microprocessor

To examine whether improved knockdown from the eSIBR backbone may be due to an increase in miRNA biogenesis, we used a previously established method for monitoring microprocessor cleavage (46). Because the amiRNA sequence is located in an exon following the GFP coding region, cleavage of the hairpin by the microprocessor separates the coding region from the polyA tail, which prevents nuclear export and destabilizes the mRNA, resulting in lowered GFP translation (Figure 4A). Thus, lowered GFP levels indicate enhanced microprocessor cleavage.

We used quantitative western blotting to measure GFP levels in COS7 cells transfected with GFP-SIBR vectors containing amiRNAs in the wtSIBR or modified SIBR backbones (Figure 4B). We compared GFP levels in cells transfected with amiRNAs in modified SIBR backbones relative to their wtSIBR counterparts and found decreased GFP levels in cultures expressing eSIBR amiRNAs, but not in cultures with amiRNAs in backbones containing

Figure 4 (next page). The eSIBR backbone increases cleavage by the microprocessor. (**A**) Schematic of microprocessor activity assay. GFP-SIBR mRNA is either exported from the nucleus to be translated or the amiRNA is cleaved by the microprocessor and the mRNA is degraded. (**B**) Representative western blots showing GFP levels in COS7 cells transfected with GFP-SIBR constructs containing the indicated amiRNAs in wild-type or modified SIBR backbones. Actin was used as a loading control. (**C**) Comparison of GFP levels measured by quantitative western blot of COS7 cells transfected with GFP-SIBR constructs carrying amiRNAs in modified backbones (bars) relative to their corresponding wtSIBR counterparts (dotted line). (**D**) Representative SIBR pri-miRNA and gapdh loading control qRT-PCR amplification plots using cDNAs synthesized from COS7 cell total RNA following transfection of hairpin nlgn3.1900 in wtSIBR or modified backbones. Insets are of the threshold cycle region of the amplification curves. (**E**) Comparison of SIBR pri-miRNA levels measured by qRT-PCR of COS7 cells transfected with GFP-SIBR constructs carrying amiRNAs in modified backbones (bars) relative to their corresponding wtSIBR counterparts (dotted line). If more than one experiment was conducted for an amiRNA sequence, the average value was used. (C) n = 16 amiRNAs, (E) n = 18 amiRNAs, **p<0.01, ***p<0.001, n.s.=not significant, one-way ANOVA with Tukey's post-hoc comparison to the wtSIBR group. Error bars represent s.e.m.

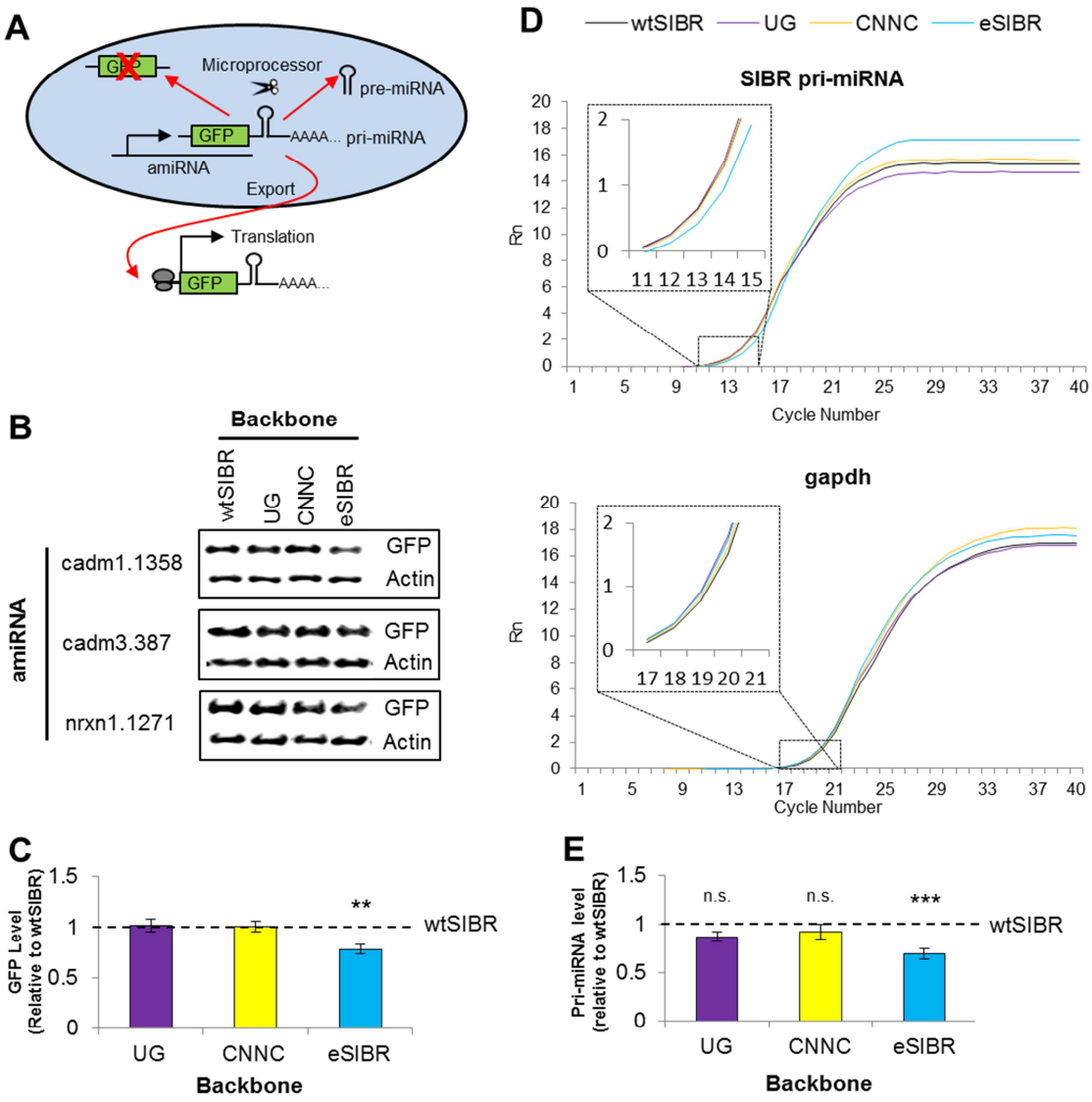

individual UG or CNNC motifs (Figure 4C). This observation suggests that increased knockdown gained from the eSIBR backbone stems from enhanced microprocessor cleavage.

To directly monitor amiRNA processing, we performed quantitative real-time PCR (qRT-PCR) to measure unprocessed pri-miRNA levels in COS7 cells transfected with GFP-SIBR vectors and compared relative pri-miRNA levels of amiRNAs expressed from the modified SIBR backbones to pri-miRNA levels of their counterparts in the wtSIBR backbone. Mirroring the results obtained by monitoring relative GFP levels, only amiRNAs expressed from the eSIBR backbone, and not backbones with a single motif, showed significantly reduced pri-miRNA levels

of ~30% (Figures 4D and 4E). Because these were overexpression experiments, the observed ~30% reduction in pri-miRNA levels due to the eSIBR modifications is not representative of single-copy kinetics and likely under-represents the increase in the amount of pre-miRNAs able to enter the RNAi pathway. Together, these results provide strong evidence that the eSIBR backbone enhances knockdown through increased microprocessor cleavage and liberation of pre-miRNA hairpins.

Chaining amiRNAs targeting different genes increases knockdown potency

One useful feature of the SIBR cassette is the ability to easily chain amiRNAs in tandem (11). To simultaneously knockdown multiple genes, we chained together amiRNA triplets in the wtSIBR or eSIBR backbones, targeting three different cadm family or nlgn family genes (e.g. cadm1, 2 and 3 or nlgn1, 2 and 3) (Figure 5A). Three unique scrambled amiRNA sequences targeting no known genes served as a control (scrambled1, 2 and 3).

We wanted to determine if chaining amiRNAs in tandem influenced their individual efficacies. Because DNA sequences can be highly homologous between gene family members, we investigated potential cross-targeting of amiRNA sequences within their gene family. We monitored knockdown of HA-reporters when co-transfected with single amiRNAs against each of the family members (Figure 5B). We found that only one amiRNA, nlgn2.1283, not only reduced HA-Neuroligin2 levels but also HA-Neuroligin3 levels, presumably due to 19/22 nucleotide homology with the target sequence. We therefore omitted HA-Neuroligin3 from subsequent analysis of linkage-based effects.

To test if multimerizing amiRNAs could alter their efficiency, we used quantitative western blotting to monitor reporter knockdown in COS7 cells co-transfected with triplet amiRNAs and their corresponding HA-reporter vectors (Figure 5C). Knockdown efficiency was measured by normalizing reporter levels to control cultures co-transfected with an empty GFP-

wtSIBR vector. Again in all cases, we found that single amiRNAs in the eSIBR backbone enhanced knockdown efficiency compared to single amiRNAs in the wtSIBR backbone and increased potency-of-knockdown ~2-fold (data not shown). Surprisingly, we found that concatenation of amiRNAs in the wtSIBR backbone targeting different genes was itself sufficient to increase knockdown efficiency for 4 of the 5 reporter constructs (Figure 5D). To compare relative effects of chaining amiRNAs across different amiRNA sequences, we calculated potency-of-knockdown for amiRNA triplets in the wtSIBR backbone compared to their corresponding single wtSIBR amiRNAs. We found that chaining wtSIBR amiRNAs significantly increased potency-of-knockdown nearly 2-fold (~1.9-fold, Figure 5E). When compared to their single eSIBR amiRNA counterparts, triple amiRNAs also increased potency-of-knockdown ~1.9-fold

Figure 5 (next page). Chaining amiRNAs targeting distinct genes increases knockdown potency. (**A**) Schematic of GFP-SIBR constructs expressing a single hairpin or triple hairpins used in this figure. Single hairpin constructs contain an amiRNA targeting a single gene. Triple hairpin constructs contain three unique amiRNA sequences targeting different genes of the same family (e.g. cadm1, 2, and 3 or nlgn1, 2 and 3) or contain three unique scrambled sequences (scrambled1, 2, and 3). (**B**) Representative western blots showing knockdown fidelity for all combinations of HA-reporter constructs co-transfected with single wtSIBR amiRNAs and a control vector containing an empty wtSIBR cassette (empty) in COS7 cells. Cross-targeting is marked by an asterisk. (**C**) Representative western blots and (**D**) quantification of reporter knockdown efficiency in COS7 cells co-transfected with GFP-SIBR constructs carrying indicated single or triple amiRNA sequences in either wtSIBR or eSIBR backbones. Knockdown percentage was calculated relative to reporter co-transfections with a control vector containing an empty wtSIBR cassette (not shown). Data for single eSIBR amiRNAs are not shown. Actin was used as a loading control. Values represent the average of 3 independent experiments. (**E**) Comparison of potency-of-knockdown for triple-amiRNA expressing constructs (bars) relative to their counterparts with single-amiRNAs in the wtSIBR backbone (dotted line) and (**F**) comparison of potency-of-knockdown for triple eSIBR amiRNA expressing constructs (bar) relative to counterparts single amiRNAs in the eSIBR backbone from experiments in (D). Values represent the average of all values for 3 independent experiments of the 5 conditions as in (D) (total n=18 per group). **p<0.01, ***p<0.001, student's two-tailed t-tests against the relative control group (dotted line). (**G**) Comparison of potency-of-knockdown for triple-amiRNA constructs in eSIBR backbones (blue bars) relative to their counterparts expressing triple-amiRNAs in the wtSIBR backbone (black bars) from data in (D). n = 3 independent experiments, *p<0.05, **p<0.01, ***p<0.001, Student's two-tailed t-test. (**H**) Comparison of pri-miRNA levels measured by qRT-PCR in COS7 cells following transfection of single and triple cadm1.1358- and nlgn2.1283-containing SIBR constructs in either the wtSIBR or eSIBR backbones. pri-miRNA levels are relative to the single wtSIBR amiRNA condition. n = 3 independent experiments, *p<0.05, **p<0.01, ***p<0.001, Student's two-tailed t-test against the single wtSIBR amiRNA condition. For all graphs, error bars represent s.e.m.

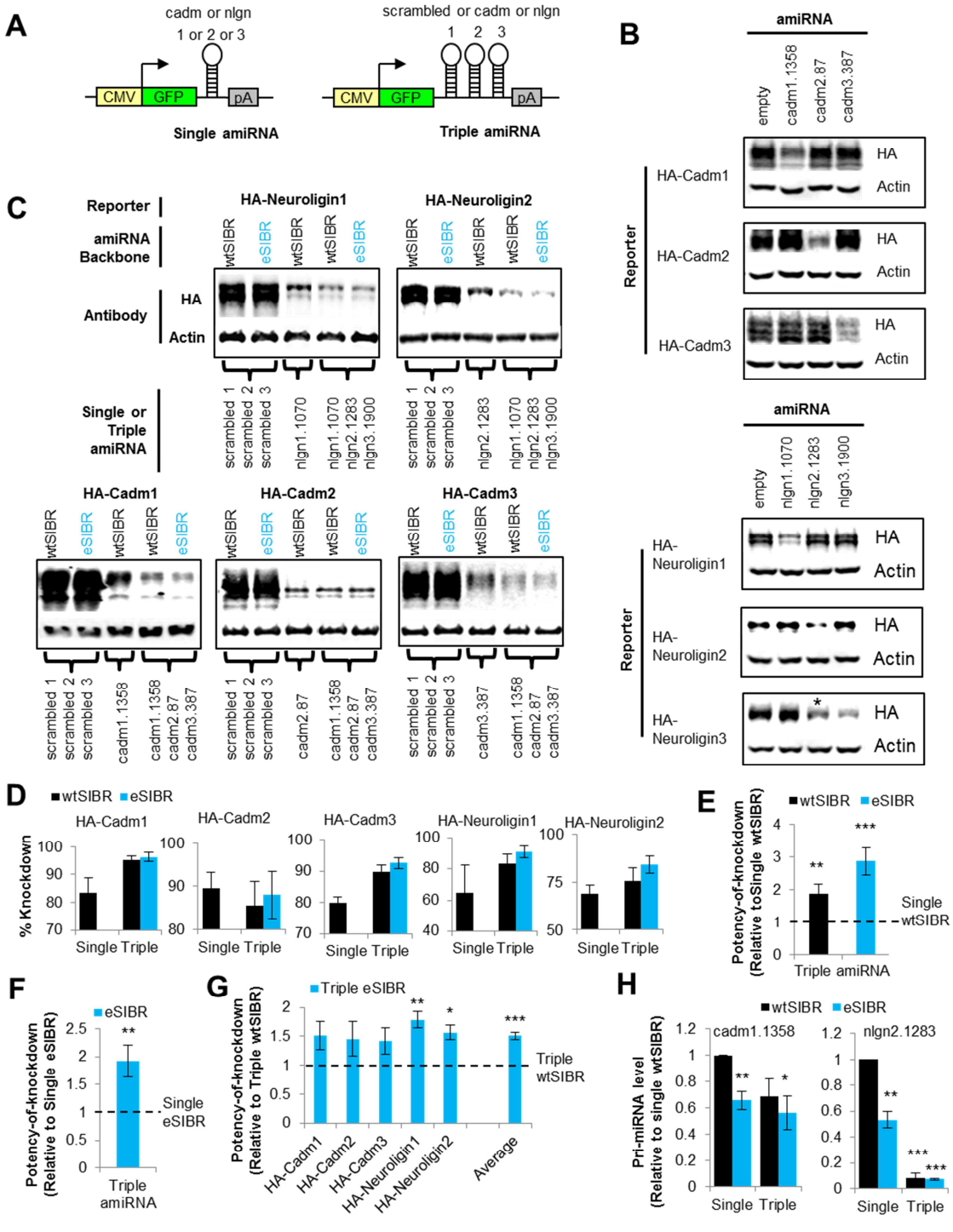
A
cadm or nlgn
1 or 2 or 3
CMV
GFP
pA
Single amiRNA
scrambled or cadm or nlgn
1 2 3
Triple amiRNA
B
amiRNA
empty
cadm1.1358
cadm2.87
cadm3.387
Reporter
HA-Cadm1
HA-Cadm2
HA-Cadm3
HA
Actin
nlgn1.1070
nlgn2.1283
nlgn3.1900
HA-Neuroligin1
HA-Neuroligin2
HA-Neuroligin3
C
Reporter
amiRNA Backbone
Antibody
wtSIBR
eSIBR
Single or Triple amiRNA
scrambled 1
scrambled 2
scrambled 3
D
wtSIBR
eSIBR
% Knockdown
Single
Triple
E
Potency-of-knockdown (Relative toSingle wtSIBR)
Triple amiRNA
F
Potency-of-knockdown (Relative to Single eSIBR)
Triple amiRNA
G
Triple eSIBR
Potency-of-knockdown (Relative to Triple wtSIBR)
Average
H
Pri-miRNA level (Relative to single wtSIBR)
cadm1.1358
nlgn2.1283

(Figure 5F), which suggests that the eSIBR backbone modifications do not interfere with chaining-based knockdown enhancement. As each amiRNA targeted distinct genes and enhanced knockdown was still observed, our results suggest a cooperative effect for miRNA biogenesis when amiRNAs are chained in close proximity.

The eSIBR backbone enhances multi-gene knockdown

To test if eSIBR amiRNAs retain their enhanced knockdown potential when concatenated, we calculated potency-of-knockdown for triplet GFP-SIBR constructs containing amiRNAs in the eSIBR backbone relative to corresponding single or triple amiRNAs in the wtSIBR backbone. When compared to their triplet wtSIBR counterparts, triplet eSIBR amiRNAs increased potency-of-knockdown in all 5 conditions, with an average enhancement of ~1.5-fold (Figure 5G), which is less than the expected 2-fold increase seen in single amiRNAs. When directly compared to their single amiRNA counterparts in the wtSIBR backbone, triplet eSIBR amiRNAs showed a nearly 3-fold increase in potency-of-knockdown (~2.9-fold, Figure 5E), which is less than the expected ~4-fold enhancement in potency-of-knockdown if both the enhancement from the eSIBR backbone and the linkage-based increase were independently additive. These two observations suggest that knockdown enhancement afforded by the eSIBR modifications is reduced when amiRNAs are multimerized. Nevertheless, these results show that chaining eSIBR amiRNAs, even when targeting distinct genes, can further boost overall knockdown potency.

Chaining-based knockdown enhancement is due to increased pri-miRNA processing

We tested if the linkage-based increase in knockdown potency due to chaining amiRNAs in tandem was also due to enhancement in microprocessor cleavage of the pri-miRNA hairpin. In order to directly compare pri-miRNA processing between single and chained amiRNAs, we

designed primers to monitor the 5'-most hairpin for both the cadm1-3 and nlgn1-3 triple constructs (cadm1.1358 and nlgn2.1283, respectively) and used qRT-PCR to measure pri-miRNA levels in COS7 cells transfected with triple amiRNAs in the wtSIBR or eSIBR backbones as well as the corresponding single amiRNAs in the wtSIBR or eSIBR backbones. We again observed a significant increase in pri-miRNA processing from single eSIBR amiRNAs compared to their wtSIBR counterparts (Figure 5H). Chaining amiRNAs decreased pri-miRNA levels for both amiRNAs, although levels were reduced much more for nlgn2.1283 than for cadm1.1358 (92% and 30% reduction, respectively, Figure 5H). For both amiRNAs, triple eSIBR constructs showed a further, but more modest decrease in pri-miRNA levels compared to triple wtSIBR counterparts (Figure 5H). These results imply that knockdown enhancement due to chaining amiRNAs is from increased microprocessor cleavage.

eSIBR boosts endogenous multi-gene knockdown potency

Next, we tested the applicability of eSIBR amiRNAs for multi-gene knockdown of endogenous proteins. We generated a lentiviral vector carrying triplet amiRNAs in the wtSIBR or eSIBR backbones which target cadm1, 2, and 3. amiRNA expression is driven by the CMV promoter and located in an intron preceding the coding region for nuclear-localized GFP (nlsGFP) (Figure 6A). We placed amiRNAs in an intron because intronic expression of amiRNAs enhances target knockdown (11). We transduced cultures of rat hippocampal neurons two days after plating (days *in vitro*, DIV) with high-titre lentivirus carrying triplet cadm amiRNAs or control triplet scrambled amiRNAs. We then used quantitative western blotting to monitor endogenous Cadm protein knockdown in 14DIV cultures (Figure 6B). We measured protein levels with antibodies against endogenous Cadm1, Cadm3 or pleio-Cadm, which recognizes Cadms 1, 2 and 3 (66), and measured knockdown efficiency by normalizing values to non-infected sister cultures (no virus) (Figure 6C). For all antibodies tested, amiRNAs in the

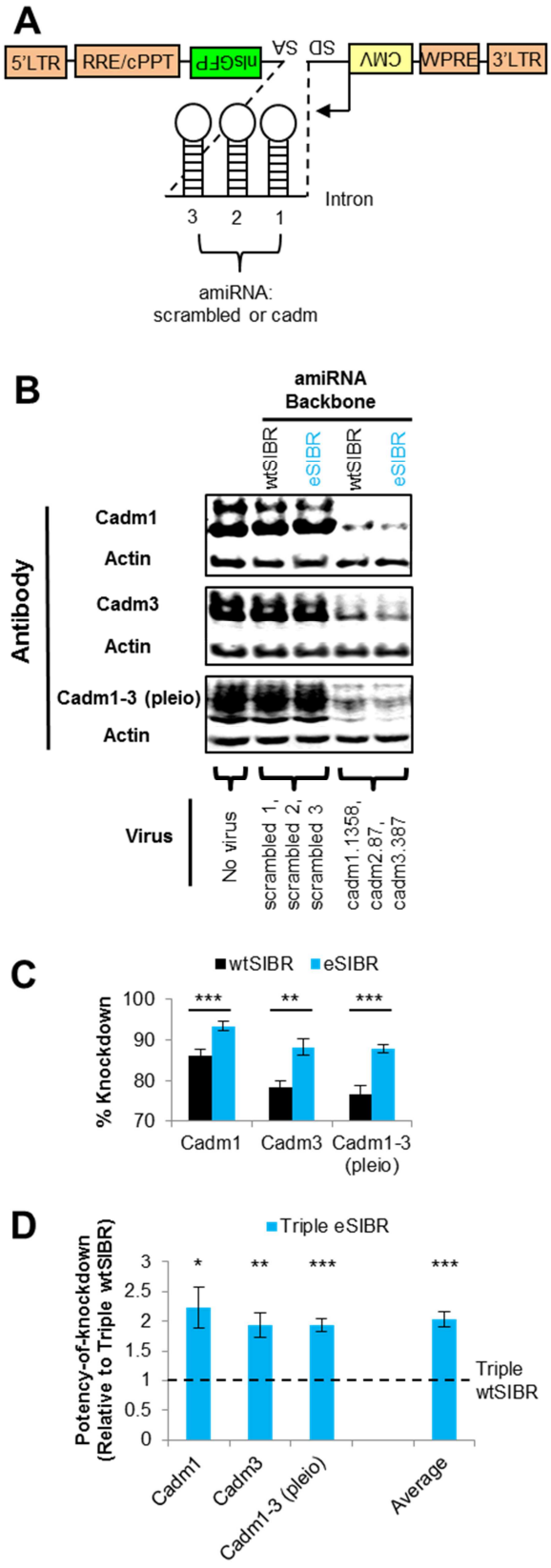

Figure 6. eSIBR enhances multi-target knockdown potency in primary neuron cultures. (**A**) Schematic of lentiviral vectors used for multiple endogenous gene knockdown. The cytomegalovirus promoter (CMV, yellow) promotes antisense-strand expression (relative to viral RNA) of amiRNAs located in an intron preceding a nuclear-localized GFP (nlsGFP, green) coding sequence. amiRNA triplets target cadm1, 2, and 3 or contain three unique scrambled sequences (scrambled1, 2, and 3). Orange boxes represent viral-specific sequences. LTR, long-terminal repeat, RRE, Rev-response element, cPPT, central polypurine tract, WPRE, woodchuck hepatitis virus posttranscriptional regulatory element, SA, splice acceptor, SD, splice donor. (**B**) Representative western blots and (**C**) quantification of endogenous Cadm family knockdown efficiency in 14DIV cultured rat hippocampal neurons transduced with viral constructs carrying the indicated amiRNA sequences in wtSIBR or eSIBR backbones. Antibodies were against Cadm1, Cadm3 or Cadm1-3 (pleio-Cadm). Knockdown percentage was calculated relative to uninfected control cultures (no virus). Actin was used as a loading control. (**D**) Comparison of endogenous Cadm potency-of-knockdown for viral vectors containing amiRNAs in eSIBR backbones (blue bars) relative to their counterparts in the wtSIBR backbone (black bars). (C) and (D) n = 4 independent experiments, *p<0.05, **p<0.01, ***p<0.001, Student's two-tailed t-test. Error bars represent s.e.m.

eSIBR backbone significantly enhanced knockdown efficiency (Figure 6C). We calculated potency-of-knockdown between triplet wtSIBR and eSIBR amiRNAs, and we found that the eSIBR backbone increased potency-of-knockdown an average ~2-fold over wtSIBR amiRNAs (Figure 6D). These results show that eSIBR is more efficient than currently-used SIBR-based vectors for endogenous multi-gene knockdown.

DISCUSSION

The use of amiRNAs have been shown throughout a diverse range of experimental contexts as an efficient means for RNAi. Despite the enormous benefits associated with amiRNAs, experimental application often suffers from insufficient target knockdown compared to other RNAi-based methods. We showed here that targeted optimization of the amiRNA SIBR backbone, termed the eSIBR scaffold, greatly enhanced the relative knockdown potency of all amiRNA sequences tested. This potent effect was due to an increase in microprocessor cleavage. When we chained eSIBR amiRNAs, even when each amiRNA targeted a unique gene, potency-of-knockdown was often enhanced more than 3-fold compared to single wtSIBR amiRNAs. Therefore, the eSIBR backbone offers great potential to boost amiRNA knockdown efficacy to comparable levels with methods such as shRNA without caveats routinely encountered with other RNAi-based techniques.

Using a large empirically-designed set of amiRNAs, we found specific sequences associated with efficient amiRNA sequences. We observed that effective sequences are highly biased for an A but against a U at guide position 10. Enrichment of A at position 10 has been previously noted for efficient shRNA and miR-30-based amiRNA sequences (55,57,67,68). Argonaute proteins in RISC cleave target mRNA between nucleotides complementary to guide strand positions 10 and 11. Bias for A at guide position 10 in effective sequences may arise from increased mRNA cleavage efficiency because a U in the mRNA complementary to guide position

10 is the preferred substrate (57). However, most previous studies also noted an enrichment of U at position 10 as well (57,67,68). In particular, studies which screened for effective amiRNA sequences using the miR-30 backbone found enrichment for both A and U at position 10 (55,69), suggesting that a bias against U at position 10 may be specific for SIBR amiRNAs. Taken together, these conflicting observations posit that differences between amiRNA expression systems, such as the loop sequence or inclusion of central mismatches, may alter primary sequences important for RNAi efficacy. Thus, our results highlight the need for more context-dependent criteria for amiRNA design.

We also observed structural criteria associated with effective amiRNAs. We and others have found that G/C content of <50% is associated with effective sequences (57,70). Specifically, our experimental average of ~40% G/C for effective amiRNAs fell precisely at the median G/C range of effective sequences in a recent, high-throughput amiRNA screen (55). We also investigated the effect of guide/passenger mismatch structure on amiRNA efficiency. We found that effective hairpins were not likely to contain an open loop mismatch and favored two mismatches separated by 3-basepaired nucleotides. We note that because COS7 cells are a monkey-derived line, the observed preference for the human mismatch structure may be due to specificities in miRNA processing machinery between species. Whether mismatch structure preference is different for SIBR-based amiRNAs in different organisms will require further investigation. Nonetheless, one should consider empirically optimizing mismatch structure when designing amiRNAs for this system if using different species. Previous studies have seen that introduction of central mismatches between the guide and passenger strands can improve knockdown efficacy in certain sequences (27,71), but to our knowledge this is the first report to systematically test preferred guide/passenger mismatch structures for an amiRNA system. Central mismatches can influence guide strand selection (72-74) as well alter loading onto functionally-distinct Ago proteins in RISC. For example, siRNAs containing central mismatches

shifts loading of guide strands from Ago2 to Ago1 in Drosophila, which alters target knockdown efficiency (75-77).

Thus, in addition to general considerations for effective RNAi design, our results suggest two important criteria for the design of effective SIBR-based amiRNAs: (1) inclusion of A and exclusion of U at guide position 10, and (2) optimization of guide/passenger mismatch structure.

One interesting trend that we noticed when comparing modified backbones containing either single UG and CNNC motifs and the eSIBR backbone, which contains both, is that while both motifs generally enhanced knockdown efficiency, the effect of single motifs on the potency of individual amiRNA sequences varied considerably. In stark contrast, combining both motifs in the eSIBR backbone reproducibly enhanced potency-of-knockdown for all 16 amiRNA sequences ~2-fold over identical sequences in the wtSIBR backbone. Because the eSIBR backbone caused such a reproducible increase in knockdown efficacy, but the effect of the individual motifs did not appear to be additive, suggests the UG and CNNC motifs are functionally linked. Indeed, we only observed increased cleavage by the microprocessor when both motifs were combined, as monitored either indirectly by GFP expression or directly by assaying pri-miRNA levels. Enhanced knockdown in the miR-30-based "miR-E" backbone by Fellmann and colleagues, which was created by reintroducing the wild-type CNNC motif, may support this notion because miR-30 already contained the basal UG motif (46). The CNNC motif was originally shown to bind the splicing factor SRp20, and more recently the DEAD-box protein DDX17, both of which associate with and can regulate microprocessor activity, although specific modes of action are not known (47,78,79). Further work will need to determine whether these regulatory mechanisms also involve the UG motif.

Our work strongly supports increased pri-miRNA processing as the causative factor of enhanced knockdown afforded by both amiRNA chaining and the eSIBR backbone modifications. Both chaining and the eSIBR backbone decreased pri-miRNA levels, as

monitored by qRT-PCR. Because an ~2-fold increase in knockdown potency was observed from both the eSIBR backbone and amiRNA chaining, we would expect an ~4-fold enhancement to potency-of-knockdown if both factors contributed independently to knockdown efficiency. However, we observed an ~3-fold increase when eSIBR amiRNAs were multimerized. Although more work is needed to determine molecular mechanisms responsible for this observation, it is possible that pri-miRNA processing efficiency hits a maximum level which is less than the maximum contribution from both the eSIBR backbone and linkage-based effect. Indeed, we found that the combination of both factors caused only a modest further increase in pri-miRNA processing as compared to much larger individual contributions from chaining or the eSIBR backbone alone. In further support of this notion, we determined that the lower than expected knockdown enhancement was not simply due to the eSIBR backbone interfering with the chaining effect; wtSIBR and eSIBR backbones similarly enhanced knockdown potency when multimerized. Interestingly, effects on processing efficiency may be cell or species-dependent, because we observed an expected ~2-fold increase in knockdown potency when comparing triple eSIBR amiRNAs to triple wtSIBR amiRNAs in cultured rat hippocampal neurons, but only observed a 1.5-fold enhancement in our COS7 cell assays.

Our results may also suggest that the eSIBR modifications or amiRNA chaining alter pri-miRNA processing kinetics. For example, the observed non-additive increase to knockdown potency from the combination of amiRNA chaining and the eSIBR backbone could be due to a reduction in pri-miRNA processing speed for eSIBR amiRNAs, but not wtSIBR amiRNAs, when concatenated. Moreover, the idea of different processing speeds could explain why 1 out of 5 amiRNAs tested (cadm2.87) did not exhibit a chaining-based enhancement of knockdown potency. For instance, it is possible that the cadm2.87 hairpin had a higher basal processing rate than the other amiRNAs which was not further increased by amiRNA chaining. More work is

needed to investigate the exact influence of amiRNA concatenation and the eSIBR backbone on miRNA processing kinetics.

We believe that the eSIBR backbone offers three distinct advantages over the miR-E scaffold (46). First, the SIBR backbone may be intrinsically superior for multi-gene RNAi. Chung and colleagues previously demonstrated that chaining identical SIBR amiRNAs can enhance knockdown efficiency (11), and we additionally observed here that concatenating amiRNAs which targeted different genes was sufficient to increase knockdown potency. While this linkage-based enhancement has been seen for at least one other amiRNA backbone (9), effects of chaining miR-30-based amiRNAs are less consistent, and may even decrease amiRNA efficacy (40,80,81). Importantly, knockdown improvement due to concatenation was retained in eSIBR amiRNAs, in addition to the enhancement provided by the backbone modifications. Taken together, these results establish the eSIBR backbone as a promising tool for multi-gene knockdown. The second advantage of the eSIBR backbone is ease of cloning compared to the miR-E backbone, which requires de-novo synthesis of a 97-mer including the amiRNA target sequence and flanking optimized scaffold region (46). The eSIBR backbone can be easily swapped to replace existing wtSIBR scaffolds by restriction enzyme digestion and ligation as described in the original report (11). Furthermore, any previously designed SIBR amiRNAs can be inserted directly into the eSIBR backbone without the need to synthesize new sequences. Third, a recent breakthrough for functional zebrafish genetics used SIBR-based amiRNAs to create the first RNAi system to cause sufficient gene knockdown in this organism (82). In the study, SIBR/mi-155-based amiRNAs vastly outperformed amiRNAs expressed from the endogenous zebrafish miR-30 backbone, which posits that SIBR-based amiRNAs may be more potent in general than amiRNAs expressed from the miR-30/E scaffolds. It will be of large interest to determine if the eSIBR backbone can further enhance knockdown in zebrafish as this

may become an invaluable tool for an organism that currently has few methods for conditional loss-of-function studies.

We offer here an outline for efficient multi-gene knockdown, from amiRNA design through implementation using the eSIBR backbone. We showed the applicability of eSIBR-based miRNAs by potently knocking down three members of a gene family in cultured neurons using a lentiviral expression system, demonstrating the eSIBR backbone as a useful tool for RNAi-based research. We believe that the eSIBR backbone holds great promise for applications which may benefit from multi-target RNAi, such as tackling functional redundancy within gene families or even gene therapy-based methods requiring simultaneous knockdown of multiple genes.

CHAPTER III

SYNCAMS FUNCTION REDUNDANTLY TO SHAPE EXCITATORY SYNAPSES

The work presented here represents unpublished co-authored material. This work was co-authored by myself, Carly Williams, Scott Stewart, Kryn Stankunas and Philip Washbourne. Carly Williams helped run many of the experiments. Scott Stewart and Kryn Stankunas developed many of the vectors for generation of lentiviral knockdown and rescue constructs. Philip Washbourne contributed to the experimental design and helped with editing the manuscript. I conceived the study and experimental design, ran the majority of the experiments, analyzed the data, and wrote the paper.

INTRODUCTION

Synaptogenesis, the process of synapse formation, is thought to be initiated by physical contact of adhesion molecules located on a presynaptic axon and postsynaptic dendrite of two different neurons (for review see Garner et al., 2002; Waites et al., 2005; Washbourne 2004). In addition to holding synapses together, interaction between adhesion molecules triggers the recruitment of distinct pre- and post-synaptic components. In the case of excitatory synapses, which represent the vast majority of synapses in the mammalian central nervous system (CNS), this includes the recruitment of glutamate-filled synaptic vesicles to the presynaptic active zone as well as glutamate receptors and scaffolding molecules of the membrane-associated guanylate kinase (MAGUK) family to the postsynaptic density (PSD). The nectin-like synaptic cell adhesion molecule (SynCAM) family has joined an ever-growing list of adhesion molecules known to be important for synapse formation including neurexin/neuroligins, cadherins, NCAM, and Ephrin-EphR complexes (Tallafuss et al., 2010).

Genetically, genome-wide association studies strongly link SynCAMs, encoded by the cell adhesion molecule (CADM) genes (Thomas et al., 2008), to the occurrence of many higher-order cognitive disorders such as autism (Zhiling et al., 2008), major depressive disorders and risk of suicide (Benton et al., 2012; Niculescu et al., 2015), and bipolar disorder (Redei et al., 2014). Additionally, SynCAM1 knockout mice have learning and memory deficits (Robbins et al., 2010) and display behaviors which parallel symptoms of autism and attention deficit hyperactivity disorder (ADHD) (Sandau et al., 2012; Takayanagi et al., 2010). A better understanding of SynCAM function may prove useful for the treatment of these disorders.

Mechanistically, SynCAMs display a potent ability to induce the formation of functional presynaptic terminals when presented to axons *in vitro* (Biederer et al., 2002; Czondor et al., 2013; Hoy et al., 2009; Sara et al., 2005). Beyond this ability, there is little agreement in the field about specific synaptogenic functions ascribed to SynCAMs. For example, overexpression of SynCAM1 *in vivo* increased hippocampal excitatory synapse density (Robbins et al., 2010), but overexpression experiments in cultured neurons are contradictory with some reports showing an increase in synapse density (Cheadle and Biederer, 2012), while others reports, even from the same group, display no change (Burton et al., 2012; Fogel et al., 2007; Sara et al., 2005). Loss-of-function experiments have similarly contradictory results. Again *in vivo*, one study showed SynCAM1 knockout causes a small, but significant, decrease in spine and synapse density (Robbins et al., 2010). Subsequent reports in culture with SynCAM1 knockout neurons or RNAi-mediated SynCAM1 knockdown show conflicting effects on synapse density directly quantified by immunostaining for synaptic markers or indirectly measured through spine density (Burton et al., 2012; Cheadle and Biederer, 2012). Despite a clear synaptogenic potential, the molecular mechanisms that SynCAMs use to form synapses remain unclear, and there is a need to reconcile gain- and loss-of-function phenotypes in order to characterize synaptic functions of SynCAMs.

A possible reason for a lack of mechanistic understanding of SynCAM function, and for studies of synaptogenic processes in general, is functional redundancy. In many cases characterizing molecular functions at synapses is precluded not only by massive overlap in signaling pathways and binding partners (Dalva et al., 2007; Kim and Sheng, 2004; Scheiffele, 2003), but also by functional redundancy within gene families themselves. Importantly, compensatory functions from additional family members or different adhesion molecules may hide crucial synaptic functions when manipulating individual genes. Indeed, redundancy has been observed for neurexins, neuroligins, calsyntenins, and MAGUKs, such that for each of these gene families protein reduction of at least three members is necessary to observe certain synaptic phenotypes (Gokce and Sudhof, 2013; Levy et al., 2015; Shipman et al., 2011; Um et al., 2014). SynCAMs have four members (SynCAM1-4) that can form homo- or hetero-philic interactions in *trans* across the synaptic cleft, and are also among the first proteins found at a nascent synapse (Biederer, 2006; Fogel et al., 2007; Stagi et al., 2010). SynCAM1-3 have been found both pre- and post-synaptically at excitatory synapses (Cheadle and Biederer, 2012; Fogel et al., 2007; Shu et al., 2011) and make up approximately 0.5% of the protein content of a synapse (Robbins et al., 2010). The short intracellular regions of SynCAM1, 2 and 3, which are necessary for synaptogenic activity (Biederer et al., 2002; Sara et al., 2005), contain remarkably conserved single FERM and PDZ binding motifs and most likely interact with the same proteins during development (Biederer, 2006). Therefore compensation between SynCAMs may hinder their functional characterization at synapses.

Here we present a novel analysis method for overcoming functional redundancy which we call Mosaic Expression using Differentially-Localized Reporters (MEDLR). MEDLR uses combinatorial lentiviral transgenesis with different subcellularly-localized GFP reporters linked to gene knockdown or overexpression constructs. Multi-gene knockdown is achieved through the use of RNAi targeting sequences expressed from enhanced artificial miRNA (amiRNAs)

backbones which are chained in tandem in the same expression cassette (Fowler et al., 2015), making MEDLR especially suitable to address functional redundancy. This method generates traceable mosaic gene expression patterns and allows dissection of cell-autonomous from non cell-autonomous effects. Crucially, in neurons this allows the differentiation of pre-and post-synaptic effects due to genetic gain or loss-of-function. Using MEDLR, we find that SynCAMs are necessary for and function redundantly to set excitatory synapse number and size in cultured rat hippocampal neurons through a postsynaptic mechanism.

RESULTS

Generation of lentiviral gain- and loss-of-function constructs

In an attempt to reconcile gain- and loss-of-function effects for multiple SynCAM protein isoforms, we developed a rapid method to generate lentiviral knockdown and overexpression vectors based on Multi-site Gateway (Invitrogen) recombination cloning. This method allows for insertion of up to three independent elements in series from 5', middle, and 3' entry vectors into a lentiviral destination vector containing additional sequences necessary for production and efficient packing of viral RNA transcripts into mature lentiviral particles via LR-clonase recombination reactions (Figure 1A). The lentiviral destination vector (pLentiDest_inverse) promotes viral RNA transcription in an antisense orientation compared to the inserted elements, and allows for enhanced lentiviral packaging by preventing same-strand promoter competition between the viral RSV promoter and the inserted entry elements (Schambach et al., 2006).

Lentiviral-mediated knockdown is achieved through the use of amiRNAs expressed from an enhanced synthetic inhibitory BIC/miR-155 RNA (eSIBR) backbone (Fowler et al., 2015). Importantly, these amiRNA cassettes can be chained for potent, simultaneous multi-gene knockdown, and are expressed from an intron upstream of nuclear-localized GFP (nlsGFP) which prevents amiRNA cleavage from affecting reporter expression levels. Lentiviral knockdown

vectors are generated with a minimal CMV promoter in a 5' entry vector, intronic single or chained amiRNAs in a middle entry vector, and nlsGFP in a 3' entry vector following recombination with pLentiDest_inverse (Figure 1B). These vectors allow for traceable knockdown via a nuclear GFP reporter. To label neuronal dendrites, we used a previously developed middle entry vector with membrane-targeted GFP (Kwan et al., 2007) to generate a lentiviral vector only expressing memGFP (Figure 1C).

Additionally, to generate lentiviral rescue or overexpression vectors also co-expressing the memGFP reporter, we developed new entry vectors with memGFP and the porcine teschovirus-1 2A sequence (P2A) in both the middle and 3' entry vectors for addition to rescue construct N- or C-termini, respectively (Figure 1D). This allows for 1:1 bicistronic expression of two independent proteins translated as a single polypeptide because of the "self-cleaving" ability of the P2A peptide sequence (Kim et al., 2011). Therefore, these vectors allow for traceable overexpression with a membrane-localized reporter.

Lentiviral-mediated knockdown ablates SynCAM1-3 protein expression

We created a lentiviral construct which co-expressed nlsGFP and chained eSIBR amiRNAs targeting SynCAM1, 2 and 3 (SynCAM1-3 amiRNA-nlsGFP) to test the ability of

Figure 1 (next page). Rapid generation of lentiviral knockdown and overexpression vectors.
(A) 5', middle, and 3' entry vectors are recombined in series via att recombination sequences into a lentiviral destination vector which promotes viral RNA transcription antisense to inserted elements (pLentiDest_inverse). Purple boxes represent viral-specific sequences.
(B) Lentiviral knockdown vectors are generated with a 5' CMV promoter, intronically expressed amiRNAs in a middle entry vector, and 3' nuclear-localized GFP (nlsGFP).
(C) A vector for dendrite labeling is created with CMV promoted membrane-localized GFP (memGFP).
(D). Lentiviral overexpression/rescue vectors are generated with a CMV promoter and either N- or C-terminal addition of P2A-linked memGFP to the rescue construct for bicistronic expression and dendrite labeling with memGFP. LTR, long-terminal repeat, RRE, Rev-response element, cPPT, central polypurine tract, WPRE, woodchuck hepatitis virus posttranscriptional regulatory element, ccdB, control of cell death type II toxin-antitoxin system B, CmR, chloramphenicol resistance, P2A, porcine teschovirus-1 2A sequence.

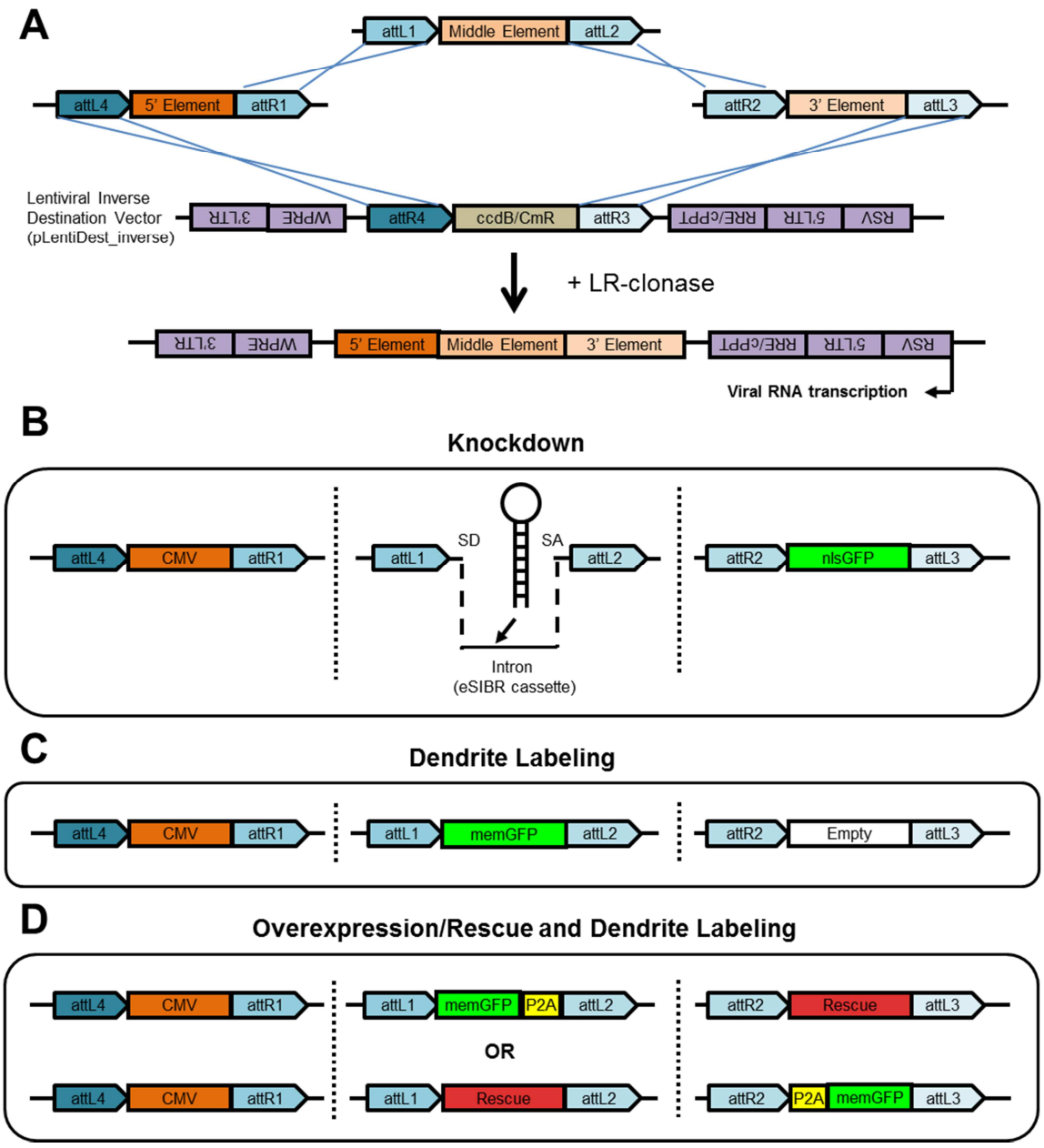

amiRNA-based lentiviral vectors to knock down SynCAM1-3 protein levels in cultured rat hippocampal neurons (Figure 2A). Neurons were infected with SynCAM1-3 amiRNA-nlsGFP at 1-2 days in vitro (DIV) with lentivirus at a multiplicity of infection (MOI) of 20 to cause saturating transduction (>99% of cells, data not shown). We used quantitative real-time PCR (qPCR) to compare cadm1-3 mRNA transcript levels in 13-15 DIV cultures, which showed

lentiviral-mediated knockdown reduced cadm1-3 levels ~75-90% compared to uninfected control cultures (Figure 2B). We also investigated knockdown potency by quantitative Western blotting using an antibody specific to the c-terminus of SynCAM1-3 (Biederer et al., 2002), but which does not recognize SynCAM4 (Fogel et al., 2007) (Figure 2C). We again infected neurons at 1-2DIV with SynCAM1-3 amiRNA-nlsGFP lentivirus or control lentivirus carrying scrambled SynCAM1-3 amiRNA guide sequences targeting no known genes (Scrambled1-3 amiRNA-nlsGFP) and compared SynCAM1-3 protein levels at 13-15DIV. At an MOI of 20, overall SynCAM1-3 levels in SynCAM1-3 amiRNA-nlsGFP infected cultures were significantly decreased by 89 ± 1% compared to cultures infected with scrambled amiRNAs (Figure 2D). Together, these results demonstrate that lentiviral amiRNA-based knockdown can robustly and simultaneously decrease the levels of SynCAM1-3 in culture.

We also monitored SynCAM1-3 knockdown by quantitative Western blotting in cultures infected with SynCAM1-3 or Scrambled1-3 amiRNA-nlsGFP at an MOI of 2 (Figure 2C), which produced sub-saturating transduction rates of 80-90% (data not shown). At this MOI, SynCAM1-3 protein levels were significantly reduced by 67 ± 3% compared to control cultures (Figure 2D). Because of the sub-saturating conditions, we speculated that the knockdown efficiency observed

---

Figure 2 (next page). amiRNA-mediated knockdown ablates SynCAM1-3 protein expression.
(A) Schematic of lentiviral knockdown vector which expresses chained amiRNAs targeting SynCAM1, 2 and 3 from an intron, followed by a nuclear-localized GFP reporter (SynCAM1-3 amiRNA-nlsGFP).
(B) Comparison of cadm1-3 mRNA levels by qRT-PCR in cultured rat hippocampal neurons relative to levels in uninfected control cultures. n=2 independent experiments.
(C) Representative quantitative Western blots and
(D) Relative SynCAM1-3 protein levels measured by quantitative Western blotting of cultured neuron following indicated amiRNA lentiviral treatments at different multiplicity of infection (MOI) relative to Scrambled1-3 amiRNA control treatments. n=4 (MOI=20) or n=2 (MOI=2) independent experiments. Actin was used as a loading control.
(E) Representative images and
(F) Quantification of relative SynCAM1-3 immunofluorescence of individual neurons cultured at low density normalized to immunofluorescent intensity of control Scrambled1-3 amiRNA treated neurons. Scrambled1-3 condition n=13 cells, SynCAM1-3 condition n=20 cells.
All error bars represent s.e.m.

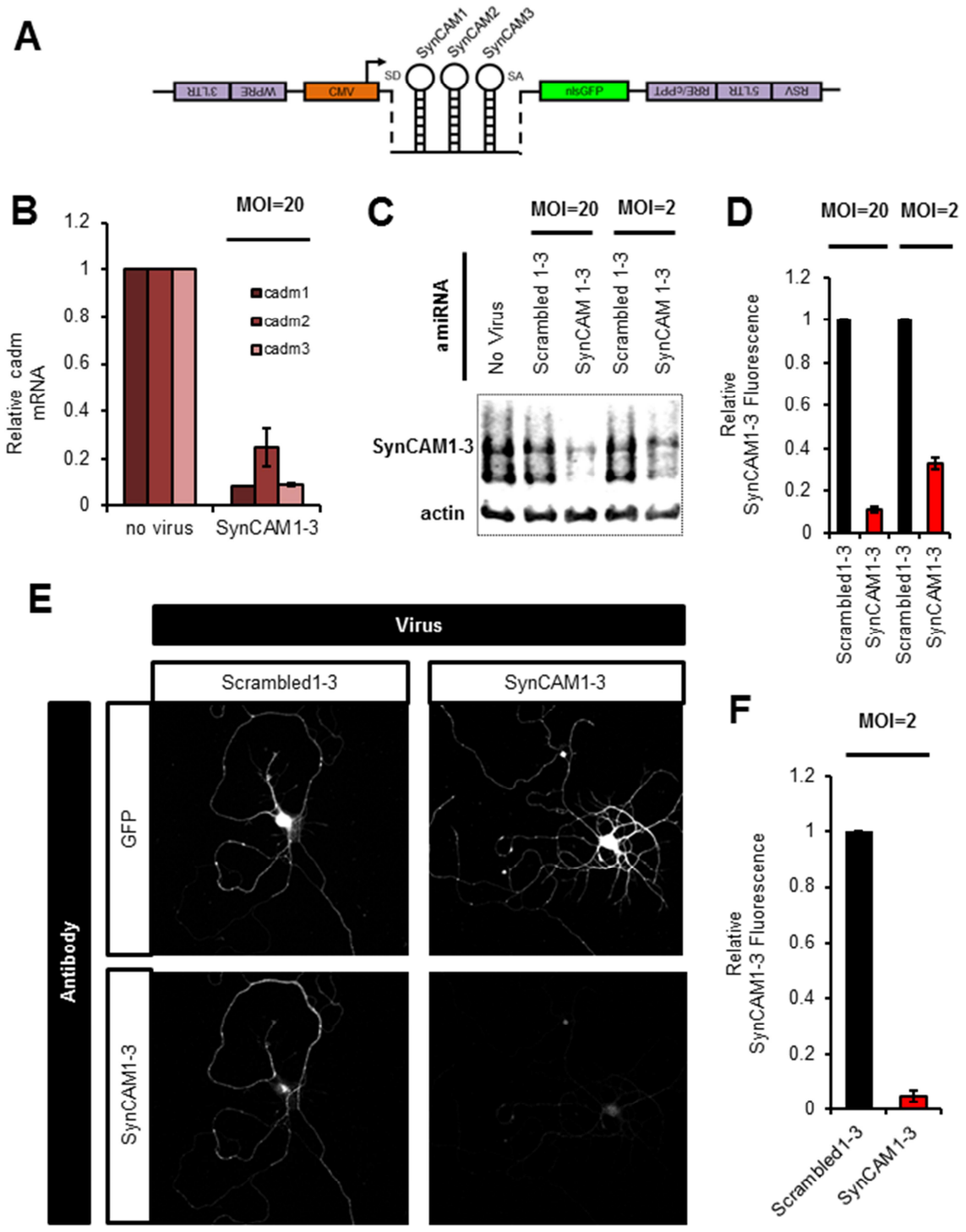
A
SynCAM1
SynCAM2
SynCAM3
SD
SA
3'LTR
WPRE
CMV
nlsGFP
RRE/cPPT
5'LTR
RSV
B
MOI=20
Relative cadm mRNA
cadm1
cadm2
cadm3
no virus
SynCAM1-3
C
MOI=20
MOI=2
amiRNA
No Virus
Scrambled 1-3
SynCAM 1-3
Scrambled 1-3
SynCAM 1-3
SynCAM1-3
actin
D
MOI=20
MOI=2
Relative SynCAM1-3 Fluorescence
Scrambled1-3
SynCAM1-3
Scrambled1-3
SynCAM1-3
E
Virus
Scrambled1-3
SynCAM1-3
Antibody
GFP
SynCAM1-3
F
MOI=2
Relative SynCAM1-3 Fluorescence
Scrambled1-3
SynCAM1-3

by Western blotting likely underrepresented knockdown efficiency in individual nlsGFP-positive cells. To address this possibility, we cultured neurons at very low density using the same sub-saturating transduction rate with SynCAM1-3 or Scrambled1-3 amiRNA-nlsGFP lentivirus. Additionally, neurons were co-infected with memGFP-only lentivirus to label individual cells for imaging. Cells were fixed and stained with the SynCAM1-3 antibody and an antibody for GFP at 13-15DIV, and overall SynCAM1-3 fluorescence in individual cells co-expressing nlsGFP and memGFP was measured (Figure 2E). When normalized to mean fluorescence levels in cells infected with Scrambled1-3 amiRNAs, SynCAM1-3 amiRNAs reduced mean SynCAM1-3 protein levels by 95 ± 2% (Figure 2F). This shows that SynCAM1-3 expression is effectively ablated by lentiviral-mediated amiRNA expression, even in sub-saturating rates of viral transduction.

Generation of an assay to compare SynCAM gain- and loss-of-function effects

We developed an assay which we termed Mosaic Expression with Differentially Localized Reporters (MEDLR) to dissect SynCAM knockdown and overexpression effects in cultured rat hippocampal neurons (Figure 3A). We infected dense neuronal cultures for imaging with knockdown lentiviral vectors at an MOI of 2 in order to achieve an ~80-90% overall transduction rate with the nlsGFP reporter. We additionally infected cells with an MOI of 0.01 with either memGFP-only lentivirus (Combination 1, Figure 3A) or memGFP rescue vectors with hemagluttanin (HA) epitope-tagged SynCAM rescue constructs (Combination 2, Figure 3A) to label a subset (~1%) of neurons with memGFP reporter for dendritic imaging. Therefore, memGFP-positive cells that were also nlsGFP-positive marked SynCAM knockdown neurons when combined with memGFP-only lentivirus. Similarly, memGFP and nlsGFP-positive cells had rescued SynCAM expression when the memGFP-HA-SynCAM rescue lentivirus was used. Crucially, because cells are transduced at a subsaturating concentration of nlsGFP-knockdown

lentivirus, this combinatorial approach allowed for the analysis of only memGFP-positive cells with SynCAM expression levels distinct from their in-condition memGFP/nlsGFP double positive counterparts. When the memGFP-only lentivirus or memGFP-HA-SynCAM rescue lentivirus were applied, memGFP-only positive cells therefore expressed wild type or overexpressed levels of SynCAMs, respectively. Thus, these two viral combinations generate differential mosaics of SynCAM expression with four classes (knockdown, wild type, rescue, and overexpression) which are linked to traceable subcellularly-localized GFP reporter patterns. One important consequence is that different expression levels can be compared on the same coverslip, ensuring cells were subjected to identical treatments. These advantages over traditional single-marker methods highlight MEDLR as a particularly suitable tool to directly compare gain- and loss-of-function effects in the same system.

Labeling a small subset of neurons with memGFP allowed unfettered imaging of cellular substructures, such as dendrites (Figure 3B). To compare differences in SynCAM-mediated synapse formation along dendrites, we developed a semi-automated program to pair with MEDLR which measures synaptic parameters such as synapse density, size, and intensity in cultures immunostained for pre- and post-synaptic markers (Figure 3C). Following manual selection of dendrites, this method uses per-dendrite thresholding for detection of pre- and post-synaptic puncta. Using this program, synapses are defined as co-localized regions of pre- and post-synaptic puncta (white in Merge image, Figure 3C).

Figure 3 (next page). Mosaic expression with differentially localized reporters (MEDLR).
(A) Overview of MEDLR approach. Two lentiviral combinations provide four traceable cellular populations with distinct protein expression levels.
(B) Representative 60X confocal microscopy image of MEDLR combination 1 as in (A) of cultured rat hippocampal neurons treated with Scrambled1-3 amiRNA-nlsGFP, with an individual pyramidal cell co-labled by memGFP and nlsGFP marked by a red arrowhead. White arrowheads mark nuclei in the field of view only expressing nlsGFP.
(C) Sample images of automated puncta and synapse detection from co-immunostaining for presynaptic marker Synapsin1 and postsynaptic marker PSD-95 following manual selection of an individual dendrite segment from the image in (B). Synapses are defined as the co-localized regions of pre- and post-synaptic puncta (white areas in merged image).

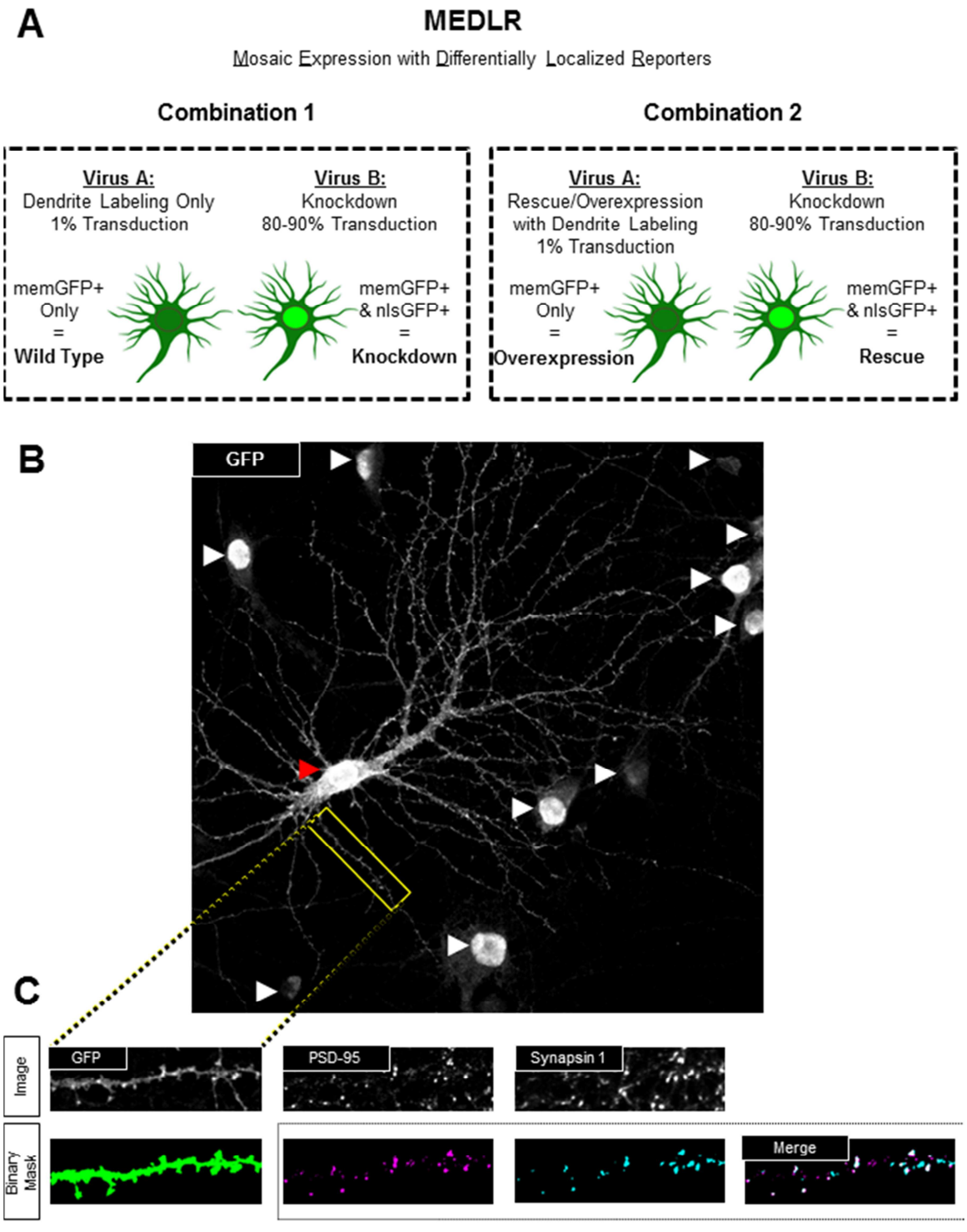
A
MEDLR
Mosaic Expression with Differentially Localized Reporters
Combination 1
Virus A:
Dendrite Labeling Only
1% Transduction
Virus B:
Knockdown
80-90% Transduction
memGFP+
Only
=
Wild Type
memGFP+
& nlsGFP+
=
Knockdown
Combination 2
Virus A:
Rescue/Overexpression
with Dendrite Labeling
1% Transduction
Virus B:
Knockdown
80-90% Transduction
memGFP+
Only
=
Overexpression
memGFP+
& nlsGFP+
=
Rescue
B
GFP
C
Image
GFP
PSD-95
Synapsin 1
Binary Mask
Merge

SynCAM1-3 knockdown reduces synapse density and increases synapse size

We used MEDLR to measure differences in synapse formation caused by SynCAM1-3 knockdown in cultured hippocampal neurons. Neurons were co-infected with memGFP-only virus for cellular labeling and with SynCAM1-3 or Scrambled1-3 amiRNA-nlsGFP lentivirus at 1-2DIV. Neurons were fixed and immunostained for GFP, the presynaptic marker Synapsin1, and the postsynaptic marker PSD-95 at 13-15DIV. Dendrites of memGFP-only and memGFP/nlsGFP double positive cells were imaged and analyzed using our puncta detection software (Figure 4A). MEDLR showed that SynCAM1-3 knockdown caused a modest, but significant, reduction of Synapsin1/PSD-95 synapse density by 16 ± 5% (Figure 4B), which is consistent with modest decreases in synapse density observed following SynCAM1 knockout (Cheadle and Biederer, 2012; Robbins et al., 2010). Furthermore, because SynCAM1-3 levels were reduced more than 95% by amiRNAs, this modest decrease suggests that SynCAM1-3 may play a role in fine-tuning synapse number. Additionally, SynCAM1-3 knockdown did not alter individual Synapsin1 or PSD-95 puncta density on dendrites (data not shown), implying that the observed phenotype is specific to transynaptic complexes with both pre- and postsynaptic structures.

Figure 4 (next page). MEDLR uncovers novel synaptic phenotypes caused by SynCAM1-3 knockdown.
(A) Representative images of automated PSD-95, Synapsin1, and synapse (merged) puncta detection for manually-selected dendrite segments of cultured hippocampal pyramidal cells using MEDLR.
(B) Relative synapse density (synaptic puncta/dendrite length) and synapse size for dendrites of pyramidal cells treated as in (A) normalized to mean values of the Scrambled1-3 amiRNA nlsGFP+ control group.
(C) Cumulative frequency and
(D) Histogram of frequencies of relative synapse density for dendrite segments of cells from treatments as in (A). Relative synapse densities were normalized to mean values of the Scrambled1-3 amiRNA nlsGFP+ control group and binned in 10% intervals from 0 to 2, which included all dendrites.
(B – D) *$p<0.05$, **$p<0.01$, pairwise student's t-tests, n=4 independent experiments (14-20 dendrites per treatment group per experiment). Error bars represent s.e.m.

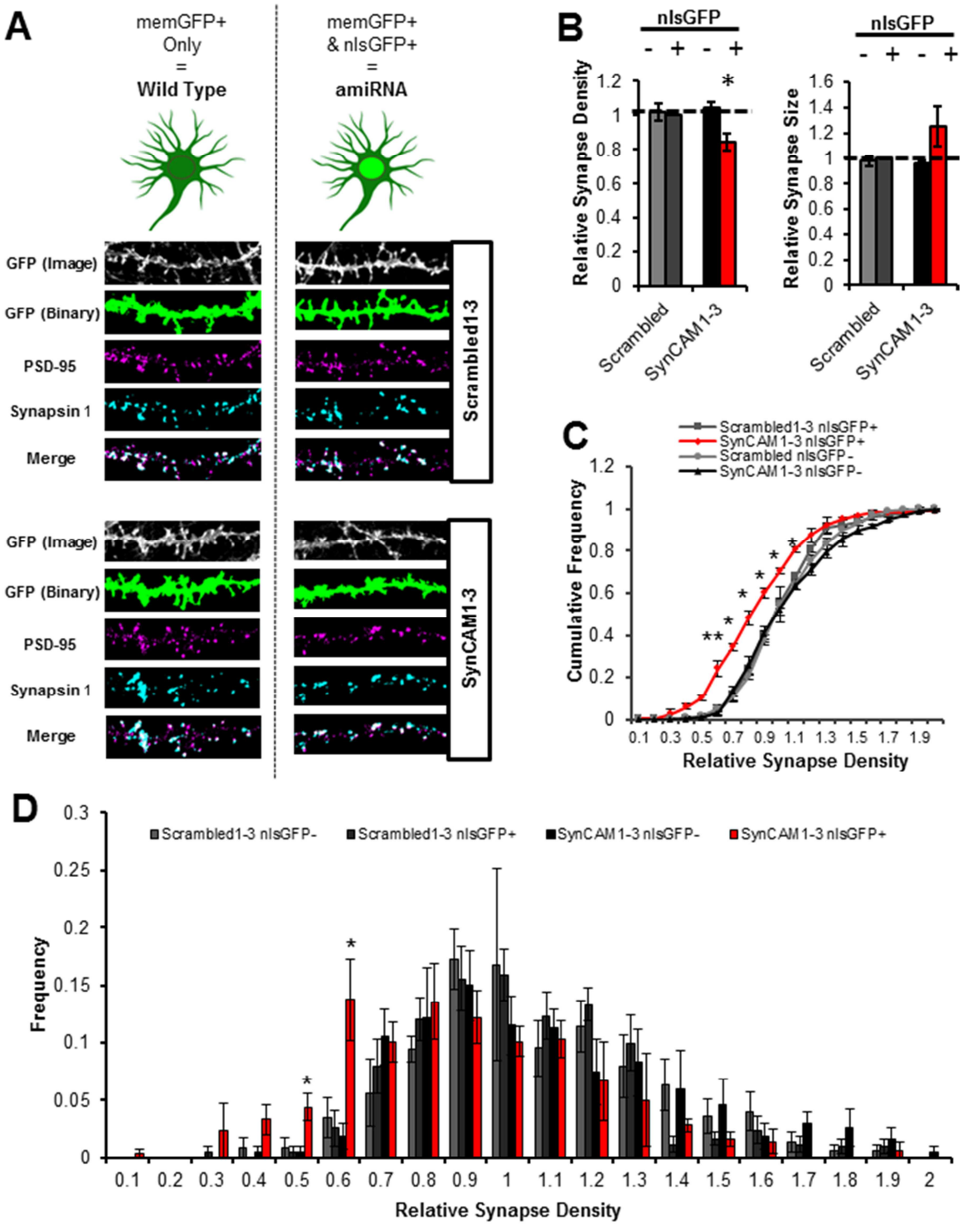
A
memGFP+
Only
=
Wild Type
memGFP+
& nlsGFP+
=
amiRNA
GFP (Image)
GFP (Binary)
PSD-95
Synapsin 1
Merge
Scrambled1-3
SynCAM1-3
B
nlsGFP
- + - +
Relative Synapse Density
Relative Synapse Size
Scrambled
SynCAM1-3
C
Scrambled1-3 nlsGFP+
SynCAM1-3 nlsGFP+
Scrambled nlsGFP-
SynCAM1-3 nlsGFP-
Cumulative Frequency
Relative Synapse Density
D
Scrambled1-3 nlsGFP-
Scrambled1-3 nlsGFP+
SynCAM1-3 nlsGFP-
SynCAM1-3 nlsGFP+
Frequency
Relative Synapse Density

Unexpectedly, we found that SynCAM1-3 knockdown caused an ~25% increase in synapse size (Figure 4B), but due to high variability in this phenotype from culture-to-culture this phenotype was not statistically significant ($p=0.17$). Nevertheless, this trend is opposite to an observed decrease in synapse size in SynCAM1 knockout mice (Robbins et al., 2010). This result may therefore indicate a new phenotype specific to SynCAM1-3 knockdown, and may suggest SynCAM isoform-specific roles in shaping excitatory synapse size. In contrast to the synaptic density phenotype, SynCAM1-3 knockdown produced non-significant increases in both PSD-95 and Synapsin1 individual puncta size (data not shown). Together, these results suggest independent mechanisms for the influence of each SynCAM on synapse density and size.

A postsynaptic, dendrite-specific mechanism for SynCAM-mediated synapse formation

When combining nlsGFP knockdown lentivirus with memGFP-only lentivirus, MEDLR affords the direct comparison of phenotypes in wild-type (memGFP positive only) and knockdown (memGFP/nlsGFP double positive) neurons in the same culture. With this specific combination, the comparison of these distinct cell populations allows discrimination of cell-autonomous from non cell-autonomous effects produced from SynCAM1-3 protein knockdown because a cell non-autonomous phenotype is expected to occur, at least partially, in the wild-type population. This is because the majority of axons impinging on wild-type (memGFP only) neurons should have reduced levels of SynCAM1-3 because they are from neurons transduced with SynCAM1-3 amiRNAs. memGFP-only expressing wild-type cells in both Scrambled1-3 and SynCAM1-3 amiRNA conditions did not show a reduction in either synapse density or size (Figure 4B), suggesting that the observed decrease in synapse density and increase in synapse size from SynCAM1-3 knockdown is a cell-autonomous effect. Importantly, these results also suggest that the observed phenotypes due to SynCAM1-3 knockdown are generated through a postsynaptic mechanism for the same reason that even though the majority of axons in culture

have reduced SynCAM1-3 levels, this does not affect their ability to form synapses onto wild-type cells in the same culture condition.

We investigated the reduced synapse density phenotype observed in SynCAM1-3 knockdown neurons in more detail by binning dendrite synapse density in 10% intervals relative to the mean synapse density in control Scrambled1-3 amiRNA memGFP/nlsGFP double positive neurons for each experiment, then averaging the binned values from 4 independent experiments. As expected, the cumulative frequency for relative synapse numbers on dendrites of SynCAM1-3 knockdown neurons shifted to significantly smaller densities compared to controls, but there was no change between control memGFP/nlsGFP double positive Scrambled1-3 amiRNA expressing cells or memGFP-only expressing wild-type cells in either amiRNA treatment condition (Figure 4C). However, when presented as a histogram, we were surprised that SynCAM1-3 knockdown did not cause a modest overall shift in relative synapse density frequency, but rather produced a sharp increase in the numbers of dendrite sections which had 40-70% less synapses than the Scrambled1-3 amiRNA control mean (Figure 4D), while leaving the overall distribution relatively unchanged. This result suggests that SynCAM1-3 selectively functions in a subset of dendrites, and therefore may represent a novel mechanism for dendrite specialization or synapse specificity.

SynCAM1-3 are functionally redundant

Finally, we generated lentiviral knockdown vectors with all possible combinations of single and double knockdowns, and tested their ability to recapitulate the SynCAM1-3 knockdown phenotypes in cultured neurons (Figure 5A). No single or double knockdown of SynCAM1-3 caused a change in synapse density or size when compared to control Scrambled1-3 amiRNA expressing neurons (Figure 5B and C). These results show that SynCAM1-3 are functionally redundant for influencing synapse density and synapse size.

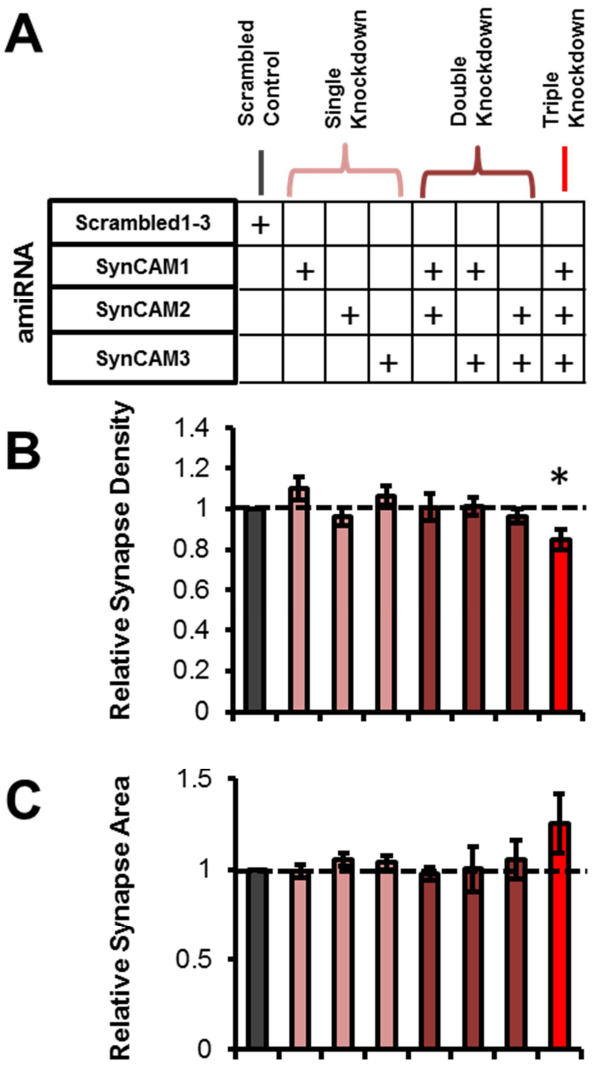

Figure 5. SynCAM1-3 are functionally redundant to set synapse density and size.
(A) Cultured neurons were infected with lentivirus carrying all possible combinations of SynCAM1-3 amiRNAs or Scrambled1-3 control amiRNAs.
(B) Relative synapse density and
(C) Relative synapse area normalized to mean values for Scrambled1-3 amiRNA treated neurons.
(B-C) $p<0.05$, pairwise student's t-tests, n=4 independent experiments for SynCAM1-3 and Scrambled1-3 amiRNA conditions, n=2 independent experiments for all others. Error bars represent s.e.m.

DISCUSSION

The SynCAM family of cell adhesion molecules has been frequently demonstrated to have an innate synaptogenic potential. However, due to inconsistent reported synaptic phenotypes of SynCAMs in gain- and loss-of-function experiments, currently there is no detailed function ascribed to SynCAMs for the process of synapse formation. A potential reason why variable phenotypes are observed is functional redundancy between SynCAM family members. Here we present a novel method, MEDLR, which we use to thoroughly characterize functional consequences of SynCAM1-3 knockdown. We find that robust knockdown (95%) of SynCAM1-3 isoforms modestly decreases synaptic density as measured by immunostaining for pre- and postsynaptic marker proteins, and that SynCAM1-3 knockdown tends to increase synaptic size. This contrasts with observed decreases in synapse size in SynCAM1 knockout mice *in vivo* (Robbins et al., 2010). Intriguingly, MEDLR showed that these phenotypes were a postsynaptic effect, which is a conclusion not attainable by single-marker knockdown analysis. Finally, we show that the three SynCAMs a function redundantly in these processes because only removal of all three produced these phenotypes. Together, these results demonstrate that SynCAM1-3 function redundantly through postsynaptic mechanisms to regulate excitatory synapse number and size.

Using MEDLR to simultaneously knock down SynCAM1-3 protein expression in cultured rat hippocampal neurons, we observed a modest, but significant, decrease in synapse density on pyramidal cell dendrites monitored by immunostaining for pre- and post-synaptic proteins. Importantly, only removal of all three SynCAMs reduced synapse density, showing that SynCAM1-3 are functionally redundant to set synapse number *in vitro*. When combined with reports of modestly decreased synapse density due to SynCAM1 knockout *in vitro* and *in vivo* (Cheadle and Biederer, 2012; Robbins et al., 2010), this result is consistent with a model in which there is a “threshold” level of SynCAMs for normal function. This model may also explain the

lack of a synaptic phenotype when using RNAi methods to knock down SynCAM1. For example, we did not see a phenotype by amiRNA-mediated knockdown of only SynCAM1, nor did a previous study which used short-hairpin RNAs (shRNAs) (Burton et al., 2012). Accordingly, functional levels of SynCAM1 may still be present due to incomplete removal of SynCAM1 through RNAi-based methods as compared to SynCAM1 knockout mice. It should be noted, however, that our amiRNA-mediated knockdown of SynCAM1 reduced >90% of mRNA levels and had a similarly robust effect on SynCAM1 protein levels (data not shown), yet no synaptic phenotypes, or even trends, were observed. Nevertheless, data presented here supports a function of SynCAMs in fine-tuning excitatory synapse density, rather than playing a fundamental role in synapse formation.

Unexpectedly, we observed that SynCAM1-3 knockdown tended to increase synapse size. SynCAM1-3 also functioned redundantly to alter synapse size, because removal of SynCAM1-3 was necessary to observe this phenotype. This is in juxtaposition to decreased synapse size reported in SynCAM1 knockout mice (Robbins et al., 2010). One explanation for this contrast may arise from inherent differences in synapse formation *in vivo* compared to in culture, as was studied here. Another possibility, however, is that synapse size is influenced differently by SynCAM gene family members such that removal of SynCAM1-3 produces an opposing effect compared to only SynCAM1 depletion. For instance, an isoform-specific binding interaction of Farp1 on the FERM motif of SynCAM1, which remains the only demonstrated SynCAM synaptic signaling mechanism, mediates SynCAM1's influence on synapse density and dendritic spine shape (Cheadle and Biederer, 2012). Therefore, it remains to be seen if SynCAM-specific mechanisms exist which regulate synapse size.

Use of MEDLR allowed us to conclude that SynCAM1-3 function postsynaptically to influence synapse number and size. This was surprising because we expected that knockdown of SynCAM1-3 in the majority of cultured neurons would generally decrease their ability to form

presynaptic terminals, since ectopic SynCAMs can potently induce presynaptic terminal formation. However, this was not observed because wild-type cells in the SynCAM1-3 knockdown cultures did not exhibit a change in synapse density or size. This instead argues that SynCAM1-3 influence excitatory synapse formation, including presynaptic development, via postsynaptic mechanisms. This notion is supported by data from the previously mentioned study which demonstrated that Farp1 functions specifically through SynCAM1 in the postsynapse to transsynaptically regulate presynaptic density (Cheadle and Biederer, 2012). A mechanism of postsynaptically-mediated transsynaptic signaling is corroborated by data presented here which show that SynCAM1-3 knockdown affects only colocalized Synapsin1/PSD-95 puncta, but does not affect individual puncta density. Taken together, these results provide strong evidence that SynCAMs function postsynaptically to mediate formation of both pre- and postsynaptic structures.

In depth analysis of the synapse density phenotype produced by SynCAM1-3 knockdown showed that there is not an overall decrease in synapse density across all dendrites, but rather that a subset of dendrites in cells lacking SynCAM1-3 have a more severe decrease in synapse density. This exciting result implies that SynCAMs function specifically in a subset of dendrites. Alternatively, this may suggest that SynCAM1-3 knockdown only produces a phenotype in a subset of pyramidal cells, as our cultures are made from a heterogeneous mixture of hippocampal neurons. Further investigation will be necessary to determine why SynCAM1-3 knockdown seems only to affect a subset of pyramidal cell dendrites.

More generally, here we offer tools for rapid generation of lentiviral knockdown and overexpression vectors and present a novel method, MEDLR, which, with a method for semiautomated analysis of immunostained synaptic markers, enables analysis following gain-and loss-of-function experiments in cultured neurons. Because the knockdown vectors make use of chained amiRNAs, these constructs are well suited to address functional redundancy. Futher,

additional controls afforded by MEDLR allow for informative comparisons of distinct cellular populations which is not possible by single-marker analysis methods. In cultured neurons, this includes comparison of cell autonomous and non cell-autonomous effects and differentiation of pre- and post-synaptic mechanisms. Together, the tools and methods presented here should help accelerate the functional characterization of synaptic proteins.

MATERIAL AND METHODS

Cloning

Lentiviral knockdown vectors. Creation of artificial miRNAs targeting SynCAM1-3 and Scrambled1-3 amiRNAs, a Multi-site Gateway middle entry vector with an intronically-expressed enhanced SIBR amiRNA cloning cassette (pME-eSIBR_intron), a 5' entry vector with a minimal CMV promoter (p5E-CMVmin) and anti-sense promoted CMV-amiRNA-nlsGFP lentiviral vectors for SynCAM1-3 knockdown was previously described (Fowler et al., 2015).

Lentiviral membrane-targeted GFP reporter. An HA-epitope tag sequence followed by a stop codon was amplified and inserted into the 3' entry vector pDONR P2R-P3 to make p3E-HA-stop. A previously described middle entry vector containing GFP with a C-terminal human H-RAS palmitoylation signal for membrane targeting (Kwan et al., 2007) was used with p5E-CMVmin and p3E-HA-stop to generate a lentiviral destination vector pLentiDest_inverse-CMVmin-memGFP. The HA epitope is not expressed because the GFP sequence used contains a stop codon and was therefore used as an "empty" 3' element to allow LR recombination.

Lentiviral rescue vectors. To generate a 3' entry vector containing the viral P2A peptide in frame to the N-terminal of memGFP (p3E-P2A-memGFP), we first cloned a p3E-P2A-MCS (multi-cloning site) vector. GFP with a C-terminal human H-RAS palmitoylation signal for membrane-targeting was amplified by PCR cloned into p3E-P2A-MCS to make p3E-P2A-memGFP. To generate a middle entry vector containing memGFP-P2A (pME-memGFP-P2A) we amplified

GFP with an N-terminal Fyn myristoylation site for dendritic membrane targeting (Kameda et al., 2008) and without a stop codon into pcDNA3 make pcDNA3-memGFP. We then inserted the P2A sequence 3' of memGFP in pcDNA3-memGFP to make pcDNA3-memGFP-P2A. memGFP-P2A was then amplified and inserted into pDONR221 to create pME-memGFP-P2A. All LR reactions were performed with a Gateway-compatible third generation lentiviral destination vector kindly provided by Dr. Kryn Stankunas (University of Oregon).

Lentivirus. Production and titering of lentivirus was previously described (Fowler et al., 2015).

Neuron culture. For single-cell SynCAM immunofluorescence comparisons, 3000 cells/well of a 12-well plate of dissociated hippocampal neurons were cultured as previously described (Fowler et al., 2015). For all other experiments, cells were cultured at a density of 100,000 cells/well of a 12-well plate. For imaging experiments, neurons were cultured on glass coverslides coated with poly-l-lysine. Neurons were infected with lentivirus at 1-2DIV. Neurons were lysed for Western blot analysis, RNA extraction, or fixed for immunostaining at 13-15 DIV. A detailed description of culturing conditions has been described previously (Fowler et al., 2015). Studies were conducted in accordance with University of Oregon Institutional Animal Care and Use Committee protocols and in compliance with NIH guidelines for the care and use of vertebrate animals.

Immunostaining. Cells on glass coverslides were fixed with 4% paraformaldehyde and 4% sucrose in PBS for 15 min at 4°C. Cells were then permeabilized for 5 min with 0.25% Triton-X100 in PBS, and blocked for 1hr at RT with blocking solution (1% Roche blocking solution (Roche), 10% BSA, 1% normal donkey serum, and 1% normal goat serum in PBS). Cells were then incubated with primary antibodies in blocking solution overnight at 4°C. Primary antibodies

and dilutions used were rabbit anti-Synapsin1 1:500 (EMD Millipore, AB1543), mouse anti-PSD-95 1:350 (Neuromab, clone K28/43), and chicken anti-GFP 1:2000 (Aves Labs, GFP-1020), and anti-SynCAM1-3 1:500 (Pierce, PA3-16744). The next day, cells were washed 3 x 5 min with PBS and incubated with secondary antibody in blocking solution for 1hr at RT. All secondary antibodies were from Jackson Laboratories and used at 1:500: goat anti-chicken Alexa Fluor 488, donkey anti-mouse or anti-rabbit Cy3, and donkey anti-rabbit Cy5. Cells were washed 3 x 5 min with PBS and mounted on slides with Fluoromount G with DAPI (Southern Biotech).

Western blotting. Quantitative western blotting for SynCAM1-3 has been previously described (Fowler et al., 2015).

qRT-PCR. First-strand cDNAs were synthesized from total RNA isolated from cultured hippocampal neurons using Superscript III reverse transcriptase (Invitrogen). cDNAs were created using oligodT primers for 50 minutes at 50°C. Primer pairs used to measure cadm mRNA levels were cadm1_F: 5'-GAAGGACAGCAGGTTTCAGC-3', cadm1_R: 5'-ACCAGGACTGTGATGGTGGT-3', cadm2_F: 5'-TCCTGATCGAATGGTTGTGA-3', cadm2_R: 5'-TGGGATCGTGTACAATGAGG-3', cadm3_f: 5'-CCTGGAGAAAAGGTGACCAA-3', cadm3_R: 5'-ATGGTTCACAGAGCACACGA-3. qRT-PCR was performed using SYBR Green reagents (Kapa Biosystems) using standard parameters on a StepOnePlus Real-Time PCR System (Applied Biosystems). Values and relative expression levels were compared using the $\Delta\Delta C_t$ method.

Imaging. Neurons were imaged on an inverted Nikon TU-2000 confocal microscope using EZ-C1 software. For single-cell comaprisons of SynCAM1-3 immunofluorescence, images were obtained using a 20X DIC objective (0.75 NA). For other experiments, images were obtained

using a 60X water immersion objective (1.2 NA) or 100X oil immersion objective (1.45 NA). For all experiments, the coverslip was scanned for cells to image using a 10X DIC objective. The presence or absence of nlsGFP was validated by visual comparison of DAPI and GFP staining. For single-cell SynCAM1-3 immunofluorescence experiments up to 20 neurons that did not overlap with neighboring cells were selected for imaging for each condition. Eight neurons were imaged for a secondary-only condition for analysis of background fluorescence. Sequential scanning for each channel (488, 543 nm) was performed and the average of three images was taken at 1024 x 1024 pixel resolution. For all other experiments, pyramidal cells were selected by morphology and cells were imaged if they had 2-3 primary or secondary basal dendrites with no further branches in a single field of view at high magnification that were visually discernable from additional GFP-positive processes and background immunofluorescence. Sequential scanning for each channel (488, 543, 633 nm) was performed and the average of three images was taken at 2048 x 2048 pixel resolution. For all experiments, images were obtained with constant pinhole, laser intensity, and detector gain settings.

Image analysis. Each confocal image channel was saved independently as a greyscale 16-bit TIFF file. For single-cell SynCAM1-3 knockdown comparisons, binary masks were made of each neuron using Image-Pro 6.3 software (Media Cybernetics) using outlines from 488nm images. Background debris was cleared from the masks manually using GIMP 2 software (The GIMP Team, 2015). SynCAM immunostaining intensity was calculated within the confines of the outline of the neuron defined by the binary masks using a custom program in MATLAB (Mathworks). The average fluorescence intensity for neurons in the secondary antibody only condition was used to measure background signal and was subtracted from the SynCAM staining intensity for each image. For dendrite analysis, using 488 nm images, individual basal dendrite segments averaging ~30 μm in length were selected and binarized manually using Image-Pro 6.3

software. Binary masks were then used in a custom MATLAB program to automatically detect and compare puncta from corresponding 543nm and 633nm images. Briefly, the program calculated the average fluorescent intensity of corresponding images in the binarized GFP region, set a threshold for including pixels in puncta detection (1.5X the mean value for each dendrite), and automatically detected puncta that were >4 continuous pixels. Only puncta that overlapped with the binarized dendrite images were counted for comparison. Overlapping pre- and postsynaptic puncta were counted as synapses. Dendrite lengths were measured manually using Image-Pro 6.3 software. Synapse density was calculated by dividing number of detected synaptic puncta by dendrite length. Synapse area was reported by our custom program.

Statistics. Two-tailed student's t-tests were performed in Microsoft Excel.

CHAPTER IV

CONCLUSIONS

The functional characterization of synaptic proteins has proven difficult for many reasons. Along with the difficulty of working with neurons, which are among the most fragile cell type, massive compensatory signaling and functional redundancy at developing synapses coupled with a lack of versatile tools and methods to generate and compare subtle changes to synapse morphology have hampered many attempts to describe molecular mechanisms of synaptogenic genes.

Throughout this dissertation, I described the development of tools to help accelerate and ease research on the mechanisms of synapse formation. In chapter II, I enhanced the knockdown potency of an artificial miRNA expression system. In addition to serving as a novel and efficient tool for multi-gene knockdown and the potential use for tackling functional redundancy at synapses, development of this enhanced amiRNA backbone led to a few unexpected discoveries. First, analysis of a large set of empirically-designed amiRNAs uncovered sequence-specific and structural features associated with efficient sequences. Further, I discovered a novel linkage-based enhancement mechanism whereby chaining amiRNAs targeting different genes increased knockdown potency through enhanced microprocessor cleavage.

In Chapter III, I adapted the enhanced amiRNA system to address functional redundancy of SynCAMs in synapse formation. Using the enhanced amiRNAs, I describe the rapid generation of lentiviral knockdown vectors. Using these vectors to knockdown SynCAM1-3 expression in cultured rat hippocampal neurons, I developed a novel combinatorial lentiviral assay with different subcellularly-localized GFP reporters to generate traceable, mosaic SynCAM expression patterns. This allowed me to separate cell autonomous and non-autonomous effects

and differentiate pre- and postsynaptic functions of SynCAM1-3. Taken together, the tools that I present represent major advancements in molecular biology techniques and should prove useful for future studies necessitating genetic loss-of-function.

Furthermore, use of these tools in Chapter III elucidated previously unknown functions of SynCAMs in synapse formation. Comparisons solidified that SynCAM1-3 function redundantly to regulate excitatory synapse density and size. Importantly, these tools allowed for the conclusion that SynCAMs function through postsynaptic mechanisms. Additionally, I determined that SynCAM effects are limited to a subset of dendrites, opening the door for further experimentation on distinct dendrite-specific functions. It will be interesting to see how these tools are expanded upon, especially the application of overexpression methods in combination with the knockdown tools developed here, and how these add to our understanding of SynCAM function. Overall, these results represent a foundational framework for the development of a cohesive SynCAM functional model.

APPENDIX

SUPPLEMENTARY FIGURES FOR CHAPTER II

Supplementary Figure S1 (next page). Changes to knockdown efficiency of hairpins expressed in modified SIBR backbones as monitored by quantitative western blotting. (**A**) Near-infrared western blot images and raw fluorescence values (A.U.) and (**B**) calculated knockdown efficiency of HA-reporters for indicated amiRNA hairpin sequences expressed from wtSIBR or modified backbones following co-transfection in COS7 cells. HA-Reporter levels were first normalized to actin loading control levels and knockdown efficiency was calculated versus the control (empty) condition. If more than one technical replicate was performed for a trial a representative replicate for that sample is shown in (**A**) and average knockdown efficiencies from 2-3 technical replicates is reported in bold font in (**B**). For gels that were not loaded in the order presented, composite blots were made from the same scan and intensity.

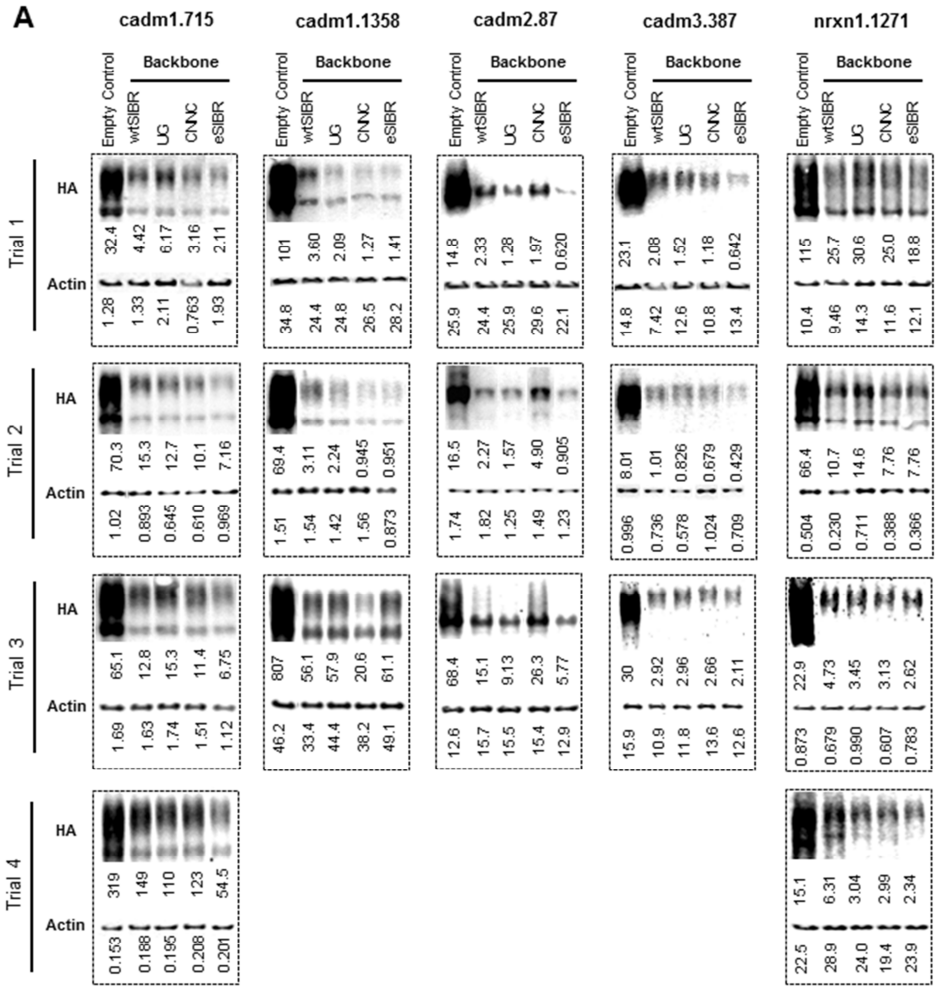

B

	cadm1.715				cadm1.1358				cadm2.87				cadm3.387				nrxn1.1271			
	wtSIBR	UG	CNNC	eSIBR	wtSIBR	UG	CNNC	eSIBR	wtSIBR	UG	CNNC	eSIBR	wtSIBR	UG	CNNC	eSIBR	wtSIBR	UG	CNNC	eSIBR
Trial 1	86.7	88.3	83.4	95.6	94.9	97.1	98.3	98.3	88.5	91.9	89.8	95.4	82.0	93.6	88.3	97.0	75.4	80.6	80.5	85.9
Trial 2	76.2	80.2	81.7	89.5	95.6	96.6	98.7	97.6	86.6	86.8	65.3	92.2	86.8	85.7	93.9	93.3	64.7	84.4	84.8	83.9
Trial 3	76.7	74.4	80.4	82.6	89.1	90.5	96.1	91.6	82.3	89.1	68.5	91.8	85.8	86.7	89.6	91.1	73.4	86.7	80.3	87.2
Trial 4	62.0	72.9	71.6	87.0													67.5	81.1	77.0	86.4
Average	75.4	79.0	79.3	88.7	93.2	94.7	97.7	95.8	85.9	89.3	74.6	93.1	84.9	88.6	90.6	93.8	70.3	83.2	80.7	85.6

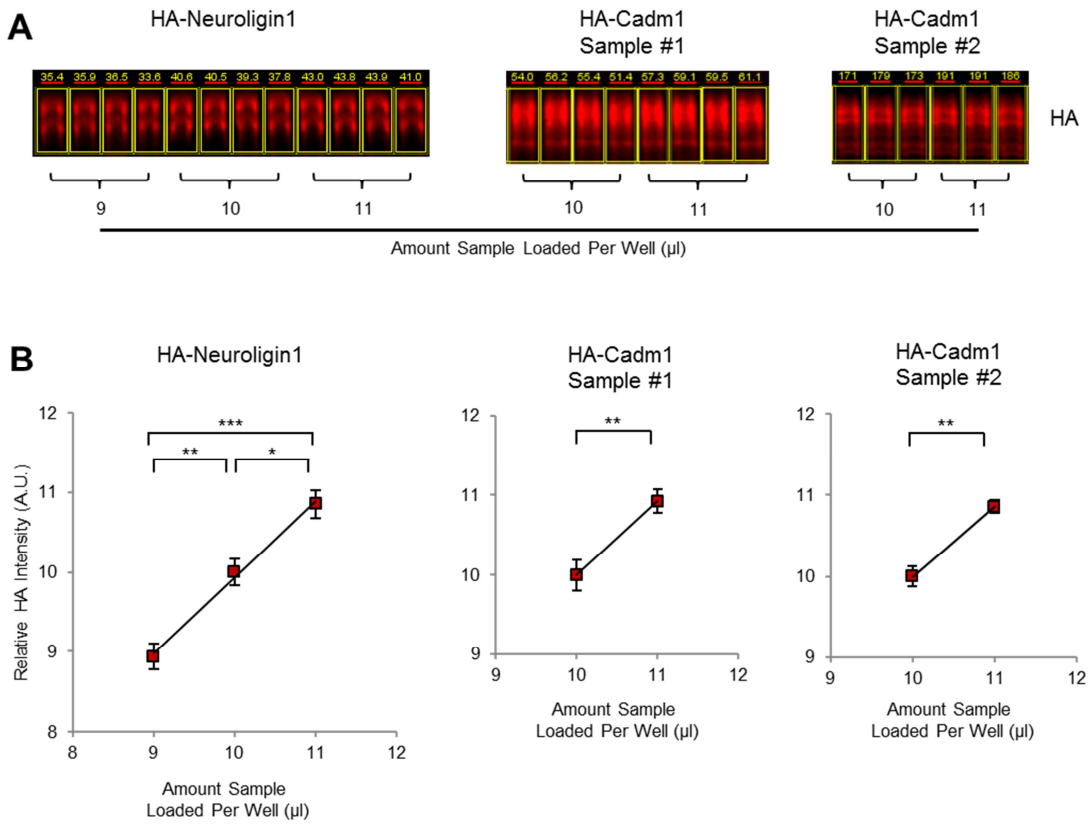

Supplementary Figure S2. Quantitative near-infrared western blotting reliably measures subtle changes in protein levels. (**A**) Near-infrared western blot images and raw fluorescence values (A.U.) and (**B**) calculated relative HA-reporter levels (A.U.) for three independent COS7 cell lysate samples following transfection with HA-Reporter. Increasing 10% amounts of lysates were loaded on gels in quadruplicate or triplicate as indicated and subjected to quantitative western blotting. Raw HA-reporter intensities were first set relative to the mean value for the 10 µl loading condition, which was then set arbitrarily at a relative HA intensity of 10 in order to illustrate the linearity of measured values. Values presented in (**B**) represent means of the quadruplicate or triplicate loadings. *p<0.05, **p<0.01, ***p<0.001, ANOVA with Tukey's post hoc pairwise comparisons for HA-Nlgn1 samples, Student's two-tailed t-test for HA-Cadm1 samples. Error bars represent S.E.M.

REFERENCES CITED

Chapter I

Akhmanova, A., and Hammer, J.A. (2010). Linking molecular motors to membrane cargo. Curr Opin Cell Biol *22*, 479-487.

Benton, C.S., Miller, B.H., Skwerer, S., Suzuki, O., Schultz, L.E., Cameron, M.D., Marron, J.S., Pletcher, M.T., and Wiltshire, T. (2012). Evaluating genetic markers and neurobiochemical analytes for fluoxetine response using a panel of mouse inbred strains. Psychopharmacology (Berl) *221*, 297-315.

Biederer, T. (2006). Bioinformatic characterization of the SynCAM family of immunoglobulin-like domain-containing adhesion molecules. Genomics *87*, 139-150.

Biederer, T., Sara, Y., Mozhayeva, M., Atasoy, D., Liu, X., Kavalali, E.T., and Sudhof, T.C. (2002). SynCAM, a synaptic adhesion molecule that drives synapse assembly. Science *297*, 1525-1531.

Breillat, C., Thoumine, O., and Choquet, D. (2007). Characterization of SynCAM surface trafficking using a SynCAM derived ligand with high homophilic binding affinity. Biochem Biophys Res Commun *359*, 655-659.

Burton, S.D., Johnson, J.W., Zeringue, H.C., and Meriney, S.D. (2012). Distinct roles of neuroligin-1 and SynCAM1 in synapse formation and function in primary hippocampal neuronal cultures. Neuroscience *215*, 1-16.

Casey, J.P., Magalhaes, T., Conroy, J.M., Regan, R., Shah, N., Anney, R., Shields, D.C., Abrahams, B.S., Almeida, J., Bacchelli, E.*, et al.* (2012). A novel approach of homozygous haplotype sharing identifies candidate genes in autism spectrum disorder. Hum Genet *131*, 565-579.

Cheadle, L., and Biederer, T. (2012). The novel synaptogenic protein Farp1 links postsynaptic cytoskeletal dynamics and transsynaptic organization. J Cell Biol *199*, 985-1001.

Czondor, K., Garcia, M., Argento, A., Constals, A., Breillat, C., Tessier, B., and Thoumine, O. (2013). Micropatterned substrates coated with neuronal adhesion molecules for high-content study of synapse formation. Nat Commun *4*, 2252.

Dalva, M.B., McClelland, A.C., and Kayser, M.S. (2007). Cell adhesion molecules: signalling functions at the synapse. Nat Rev Neurosci *8*, 206-220.

Drachman, D.A. (2005). Do we have brain to spare? Neurology *64*, 2004-2005.

Fogel, A.I., Akins, M.R., Krupp, A.J., Stagi, M., Stein, V., and Biederer, T. (2007). SynCAMs organize synapses through heterophilic adhesion. J Neurosci *27*, 12516-12530.

Fogel, A.I., Stagi, M., Perez de Arce, K., and Biederer, T. (2011). Lateral assembly of the immunoglobulin protein SynCAM 1 controls its adhesive function and instructs synapse formation. EMBO J *30*, 4728-4738.

Frei, J.A., and Stoeckli, E.T. (2014). SynCAMs extend their functions beyond the synapse. Eur J Neurosci *39*, 1752-1760.

Fujita, E., Dai, H., Tanabe, Y., Zhiling, Y., Yamagata, T., Miyakawa, T., Tanokura, M., Momoi, M.Y., and Momoi, T. (2010). Autism spectrum disorder is related to endoplasmic reticulum stress induced by mutations in the synaptic cell adhesion molecule, CADM1. Cell Death Dis *1*, e47.

Fujita, E., Tanabe, Y., Imhof, B.A., Momoi, M.Y., and Momoi, T. (2012). Cadm1-Expressing Synapses on Purkinje Cell Dendrites Are Involved in Mouse Ultrasonic Vocalization Activity. Plos One *7*.

Fukuhara, H., Kuramochi, M., Nobukuni, T., Fukami, T., Saino, M., Maruyama, T., Nomura, S., Sekiya, T., and Murakami, Y. (2001). Isolation of the TSLL1 and TSLL2 genes, members of the tumor suppressor TSLC1 gene family encoding transmembrane proteins. Oncogene *20*, 5401-5407.

Garner, C.C., Zhai, R.G., Gundelfinger, E.D., and Ziv, N.E. (2002). Molecular mechanisms of CNS synaptogenesis. Trends Neurosci *25*, 243-251.

Gokce, O., and Sudhof, T.C. (2013). Membrane-tethered monomeric neurexin LNS-domain triggers synapse formation. J Neurosci *33*, 14617-14628.

Gomyo, H., Arai, Y., Tanigami, A., Murakami, Y., Hattori, M., Hosoda, F., Arai, K., Aikawa, Y., Tsuda, H., Hirohashi, S.*, et al.* (1999). A 2-Mb sequence-ready contig map and a novel immunoglobulin superfamily gene IGSF4 in the LOH region of chromosome 11q23.2. Genomics *62*, 139-146.

Graf, E.R., Zhang, X., Jin, S.X., Linhoff, M.W., and Craig, A.M. (2004). Neurexins induce differentiation of GABA and glutamate postsynaptic specializations via neuroligins. Cell *119*, 1013-1026.

Herculano-Houzel, S. (2009). The human brain in numbers: a linearly scaled-up primate brain. Front Hum Neurosci *3*, 31.

Hoy, J.L., Constable, J.R., Vicini, S., Fu, Z., and Washbourne, P. (2009). SynCAM1 recruits NMDA receptors via protein 4.1B. Mol Cell Neurosci *42*, 466-483.

Ibrahim-Verbaas, C.A., Bressler, J., Debette, S., Schuur, M., Smith, A.V., Bis, J.C., Davies, G., Trompet, S., Smith, J.A., Wolf, C.*, et al.* (2015). GWAS for executive function and processing speed suggests involvement of the CADM2 gene. Mol Psychiatry.

Kandel, E.R. (2013). Principles of neural science, 5th edn (New York: McGraw-Hill).
Kawano, S., Ikeda, W., Kishimoto, M., Ogita, H., and Takai, Y. (2009). Silencing of ErbB3/ErbB2 signaling by immunoglobulin-like Necl-2. J Biol Chem *284*, 23793-23805.

Kim, E., and Sheng, M. (2004). PDZ domain proteins of synapses. Nat Rev Neurosci *5*, 771-781.

Kim, H.R., Jeon, B.H., Lee, H.S., Im, S.H., Araki, M., Araki, K., Yamamura, K., Choi, S.C., Park, D.S., and Jun, C.D. (2011). IGSF4 is a novel TCR zeta-chain-interacting protein that enhances TCR-mediated signaling. J Exp Med *208*, 2545-2560.

Kuramochi, M., Fukuhara, H., Nobukuni, T., Kanbe, T., Maruyama, T., Ghosh, H.P., Pletcher, M., Isomura, M., Onizuka, M., Kitamura, T.*, et al.* (2001). TSLC1 is a tumor-suppressor gene in human non-small-cell lung cancer. Nat Genet *27*, 427-430.

Levy, J.M., Chen, X., Reese, T.S., and Nicoll, R.A. (2015). Synaptic Consolidation Normalizes AMPAR Quantal Size following MAGUK Loss. Neuron *87*, 534-548.

Niculescu, A.B., Levey, D.F., Phalen, P.L., Le-Niculescu, H., Dainton, H.D., Jain, N., Belanger, E., James, A., George, S., Weber, H.*, et al.* (2015). Understanding and predicting suicidality using a combined genomic and clinical risk assessment approach. Mol Psychiatry *20*, 1266-1285.

Redei, E.E., Andrus, B.M., Kwasny, M.J., Seok, J., Cai, X., Ho, J., and Mohr, D.C. (2014). Blood transcriptomic biomarkers in adult primary care patients with major depressive disorder undergoing cognitive behavioral therapy. Transl Psychiatry *4*, e442.

Robbins, E.M., Krupp, A.J., Perez de Arce, K., Ghosh, A.K., Fogel, A.I., Boucard, A., Sudhof, T.C., Stein, V., and Biederer, T. (2010). SynCAM 1 adhesion dynamically regulates synapse number and impacts plasticity and learning. Neuron *68*, 894-906.
Ryan, T.J., and Grant, S.G. (2009). The origin and evolution of synapses. Nat Rev Neurosci *10*, 701-712.

Sandau, U.S., Alderman, Z., Corfas, G., Ojeda, S.R., and Raber, J. (2012). Astrocyte-specific disruption of SynCAM1 signaling results in ADHD-like behavioral manifestations. PLoS One *7*, e36424.

Sara, Y., Biederer, T., Atasoy, D., Chubykin, A., Mozhayeva, M.G., Sudhof, T.C., and Kavalali, E.T. (2005). Selective capability of SynCAM and neuroligin for functional synapse assembly. J Neurosci *25*, 260-270.

Scheiffele, P. (2003). Cell-cell signaling during synapse formation in the CNS. Annu Rev Neurosci *26*, 485-508.

Schlager, M.A., and Hoogenraad, C.C. (2009). Basic mechanisms for recognition and transport of synaptic cargos. Mol Brain *2*.

Shipman, S.L., Schnell, E., Hirai, T., Chen, B.S., Roche, K.W., and Nicoll, R.A. (2011). Functional dependence of neuroligin on a new non-PDZ intracellular domain. Nat Neurosci *14*, 718-726.

Stagi, M., Fogel, A.I., and Biederer, T. (2010). SynCAM 1 participates in axo-dendritic contact assembly and shapes neuronal growth cones. Proc Natl Acad Sci U S A *107*, 7568-7573.

Takayanagi, Y., Fujita, E., Yu, Z., Yamagata, T., Momoi, M.Y., Momoi, T., and Onaka, T. (2010). Impairment of social and emotional behaviors in Cadm1-knockout mice. Biochem Biophys Res Commun *396*, 703-708.

Tallafuss, A., Constable, J.R., and Washbourne, P. (2010). Organization of central synapses by adhesion molecules. Eur J Neurosci *32*, 198-206.

Thomas, L.A., Akins, M.R., and Biederer, T. (2008). Expression and adhesion profiles of SynCAM molecules indicate distinct neuronal functions. J Comp Neurol *510*, 47-67.

Um, J.W., Pramanik, G., Ko, J.S., Song, M.Y., Lee, D., Kim, H., Park, K.S., Sudhof, T.C., Tabuchi, K., and Ko, J. (2014). Calsyntenins function as synaptogenic adhesion molecules in concert with neurexins. Cell Rep *6*, 1096-1109.

Urase, K., Soyama, A., Fujita, E., and Momoi, T. (2001). Expression of RA175 mRNA, a new member of the immunoglobulin superfamily, in developing mouse brain. Neuroreport *12*, 3217-3221.

Waites, C.L., Craig, A.M., and Garner, C.C. (2005). Mechanisms of vertebrate synaptogenesis. Annu Rev Neurosci *28*, 251-274.

Wakayama, T., Ohashi, K., Mizuno, K., and Iseki, S. (2001). Cloning and characterization of a novel mouse immunoglobulin superfamily gene expressed in early spermatogenic cells. Mol Reprod Dev *60*, 158-164.

Washbourne, P., Dityatev, A., Scheiffele, P., Biederer, T., Weiner, J.A., Christopherson, K.S., and El-Husseini, A. (2004). Cell adhesion molecules in synapse formation. J Neurosci *24*, 9244-9249.

Zhiling, Y., Fujita, E., Tanabe, Y., Yamagata, T., Momoi, T., and Momoi, M.Y. (2008). Mutations in the gene encoding CADM1 are associated with autism spectrum disorder. Biochem Biophys Res Commun *377*, 926-929.

Chapter II

1. Fellmann, C. and Lowe, S.W. (2014) Stable RNA interference rules for silencing. *Nat. Cell Biol.*, **16**, 10-18.

2. Krol, J., Loedige, I. and Filipowicz, W. (2010) The widespread regulation of microRNA biogenesis, function and decay. *Nat. Rev. Genet.*, **11**, 597-610.

3. Ha, M. and Kim, V.N. (2014) Regulation of microRNA biogenesis. *Nat. Rev. Mol. Cell Biol.*, **15**, 509-524.

4. Filipowicz, W., Bhattacharyya, S.N. and Sonenberg, N. (2008) Mechanisms of post-transcriptional regulation by microRNAs: are the answers in sight? *Nat. Rev. Genet.*, **9**, 102-114.

5. Aagaard, L.A., Zhang, J., von Eije, K.J., Li, H., Saetrom, P., Amarzguioui, M. and Rossi, J.J. (2008) Engineering and optimization of the miR-106b cluster for ectopic expression of multiplexed anti-HIV RNAs. *Gene Ther.*, **15**, 1536-1549.

6. Yue, J., Sheng, Y., Ren, A. and Penmatsa, S. (2010) A miR-21 hairpin structure-based gene knockdown vector. *Biochem. Biophys. Res. Commun.*, **394**, 667-672.

7. Chang, K., Marran, K., Valentine, A. and Hannon, G.J. (2014) Generation of transgenic Drosophila expressing shRNAs in the miR-1 backbone. *Cold Spring Harb Protoc*, **2014**.

8. Yang, J.S., Maurin, T., Robine, N., Rasmussen, K.D., Jeffrey, K.L., Chandwani, R., Papapetrou, E.P., Sadelain, M., O'Carroll, D. and Lai, E.C. (2010) Conserved vertebrate mir-451 provides a platform for Dicer-independent, Ago2-mediated microRNA biogenesis. *Proc Natl Acad Sci U S A*, **107**, 15163-15168.

9. Liu, Y.P., Haasnoot, J., ter Brake, O., Berkhout, B. and Konstantinova, P. (2008) Inhibition of HIV-1 by multiple siRNAs expressed from a single microRNA polycistron. *Nucleic Acids Res.*, **36**, 2811-2824.

10. Chen, S.C., Stern, P., Guo, Z. and Chen, J. (2011) Expression of multiple artificial microRNAs from a chicken miRNA126-based lentiviral vector. *PLoS One*, **6**, e22437.

11. Chung, K.H., Hart, C.C., Al-Bassam, S., Avery, A., Taylor, J., Patel, P.D., Vojtek, A.B. and Turner, D.L. (2006) Polycistronic RNA polymerase II expression vectors for RNA interference based on BIC/miR-155. *Nucleic Acids Res.*, **34**, e53.

12. Zeng, Y., Wagner, E.J. and Cullen, B.R. (2002) Both natural and designed micro RNAs can inhibit the expression of cognate mRNAs when expressed in human cells. *Mol. Cell*, **9**, 1327-1333.

13. Boudreau, R.L., Monteys, A.M. and Davidson, B.L. (2008) Minimizing variables among hairpin-based RNAi vectors reveals the potency of shRNAs. *RNA*, **14**, 1834-1844.

14. Silva, J.M., Li, M.Z., Chang, K., Ge, W., Golding, M.C., Rickles, R.J., Siolas, D., Hu, G., Paddison, P.J., Schlabach, M.R. *et al.* (2005) Second-generation shRNA libraries covering the mouse and human genomes. *Nat. Genet.*, **37**, 1281-1288.

15. Boden, D., Pusch, O., Silbermann, R., Lee, F., Tucker, L. and Ramratnam, B. (2004) Enhanced gene silencing of HIV-1 specific siRNA using microRNA designed hairpins. *Nucleic Acids Res.*, **32**, 1154-1158.

16. Lebbink, R.J., Lowe, M., Chan, T., Khine, H., Wang, X. and McManus, M.T. (2011) Polymerase II promoter strength determines efficacy of microRNA adapted shRNAs. *PLoS One*, **6**, e26213.

17. Grimm, D., Wang, L., Lee, J.S., Schurmann, N., Gu, S., Borner, K., Storm, T.A. and Kay, M.A. (2010) Argonaute proteins are key determinants of RNAi efficacy, toxicity, and persistence in the adult mouse liver. *J. Clin. Invest.*, **120**, 3106-3119.

18. Kanasty, R.L., Whitehead, K.A., Vegas, A.J. and Anderson, D.G. (2012) Action and reaction: the biological response to siRNA and its delivery vehicles. *Mol. Ther.*, **20**, 513-524.

19. Snove, O., Jr. and Rossi, J.J. (2006) Toxicity in mice expressing short hairpin RNAs gives new insight into RNAi. *Genome Biol*, **7**, 231.

20. Grimm, D., Streetz, K.L., Jopling, C.L., Storm, T.A., Pandey, K., Davis, C.R., Marion, P., Salazar, F. and Kay, M.A. (2006) Fatality in mice due to oversaturation of cellular microRNA/short hairpin RNA pathways. *Nature*, **441**, 537-541.

21. Castanotto, D., Sakurai, K., Lingeman, R., Li, H., Shively, L., Aagaard, L., Soifer, H., Gatignol, A., Riggs, A. and Rossi, J.J. (2007) Combinatorial delivery of small interfering RNAs reduces RNAi efficacy by selective incorporation into RISC. *Nucleic Acids Res.*, **35**, 5154-5164.

22. Amendola, M., Passerini, L., Pucci, F., Gentner, B., Bacchetta, R. and Naldini, L. (2009) Regulated and multiple miRNA and siRNA delivery into primary cells by a lentiviral platform. *Mol. Ther.*, **17**, 1039-1052.

23. McBride, J.L., Boudreau, R.L., Harper, S.Q., Staber, P.D., Monteys, A.M., Martins, I., Gilmore, B.L., Burstein, H., Peluso, R.W., Polisky, B. *et al.* (2008) Artificial miRNAs mitigate shRNA-mediated toxicity in the brain: implications for the therapeutic development of RNAi. *Proc Natl Acad Sci U S A*, **105**, 5868-5873.

24. Boudreau, R.L., Martins, I. and Davidson, B.L. (2009) Artificial microRNAs as siRNA shuttles: improved safety as compared to shRNAs in vitro and in vivo. *Mol. Ther.*, **17**, 169-175.

25. Giering, J.C., Grimm, D., Storm, T.A. and Kay, M.A. (2008) Expression of shRNA from a tissue-specific pol II promoter is an effective and safe RNAi therapeutic. *Mol. Ther.*, **16**, 1630-1636.

26. Myburgh, R., Cherpin, O., Schlaepfer, E., Rehrauer, H., Speck, R.F., Krause, K.H. and Salmon, P. (2014) Optimization of Critical Hairpin Features Allows miRNA-based Gene Knockdown Upon Single-copy Transduction. *Mol Ther Nucleic Acids*, **3**, e207.

27. Wu, H., Ma, H., Ye, C., Ramirez, D., Chen, S., Montoya, J., Shankar, P., Wang, X.A. and Manjunath, N. (2011) Improved siRNA/shRNA functionality by mismatched duplex. *PLoS One*, **6**, e28580.

28. Judge, A.D., Bola, G., Lee, A.C. and MacLachlan, I. (2006) Design of noninflammatory synthetic siRNA mediating potent gene silencing in vivo. *Mol. Ther.*, **13**, 494-505.

29. Judge, A.D., Sood, V., Shaw, J.R., Fang, D., McClintock, K. and MacLachlan, I. (2005) Sequence-dependent stimulation of the mammalian innate immune response by synthetic siRNA. *Nat. Biotechnol.*, **23**, 457-462.

30. Cao, W., Hunter, R., Strnatka, D., McQueen, C.A. and Erickson, R.P. (2005) DNA constructs designed to produce short hairpin, interfering RNAs in transgenic mice sometimes show early lethality and an interferon response. *J. Appl. Genet.*, **46**, 217-225.

31. Alvarez, V.A., Ridenour, D.A. and Sabatini, B.L. (2006) Retraction of synapses and dendritic spines induced by off-target effects of RNA interference. *J. Neurosci.*, **26**, 7820-7825.

32. Bridge, A.J., Pebernard, S., Ducraux, A., Nicoulaz, A.L. and Iggo, R. (2003) Induction of an interferon response by RNAi vectors in mammalian cells. *Nat. Genet.*, **34**, 263-264.

33. Sledz, C.A., Holko, M., de Veer, M.J., Silverman, R.H. and Williams, B.R. (2003) Activation of the interferon system by short-interfering RNAs. *Nat. Cell Biol.*, **5**, 834-839.

34. Bauer, M., Kinkl, N., Meixner, A., Kremmer, E., Riemenschneider, M., Forstl, H., Gasser, T. and Ueffing, M. (2009) Prevention of interferon-stimulated gene expression using microRNA-designed hairpins. *Gene Ther.*, **16**, 142-147.

35. Nielsen, T.T., Marion, I., Hasholt, L. and Lundberg, C. (2009) Neuron-specific RNA interference using lentiviral vectors. *J. Gene Med.*, **11**, 559-569.

36. Shin, K.J., Wall, E.A., Zavzavadjian, J.R., Santat, L.A., Liu, J., Hwang, J.I., Rebres, R., Roach, T., Seaman, W., Simon, M.I. *et al.* (2006) A single lentiviral vector platform for microRNA-based conditional RNA interference and coordinated transgene expression. *Proc Natl Acad Sci U S A*, **103**, 13759-13764.

37. Stegmeier, F., Hu, G., Rickles, R.J., Hannon, G.J. and Elledge, S.J. (2005) A lentiviral microRNA-based system for single-copy polymerase II-regulated RNA interference in mammalian cells. *Proc Natl Acad Sci U S A*, **102**, 13212-13217.

38. Du, G., Yonekubo, J., Zeng, Y., Osisami, M. and Frohman, M.A. (2006) Design of expression vectors for RNA interference based on miRNAs and RNA splicing. *FEBS J.*, **273**, 5421-5427.

39. Hu, T., Fu, Q., Chen, P., Ma, L., Sin, O. and Guo, D. (2009) Construction of an artificial MicroRNA expression vector for simultaneous inhibition of multiple genes in mammalian cells. *Int J Mol Sci*, **10**, 2158-2168.

40. Sun, D., Melegari, M., Sridhar, S., Rogler, C.E. and Zhu, L. (2006) Multi-miRNA hairpin method that improves gene knockdown efficiency and provides linked multi-gene knockdown. *BioTechniques*, **41**, 59-63.

41. Barbaric, I., Miller, G. and Dear, T.N. (2007) Appearances can be deceiving: phenotypes of knockout mice. *Brief Funct Genomic Proteomic*, **6**, 91-103.

42. Grimm, D. and Kay, M.A. (2007) Combinatorial RNAi: a winning strategy for the race against evolving targets? *Mol. Ther.*, **15**, 878-888.

43. Herrera-Carrillo, E. and Berkhout, B. (2015) The impact of HIV-1 genetic diversity on the efficacy of a combinatorial RNAi-based gene therapy. *Gene Ther.*

44. Aagaard, L. and Rossi, J.J. (2007) RNAi therapeutics: principles, prospects and challenges. *Adv Drug Deliv Rev*, **59**, 75-86.

45. Wang, S.L., Yao, H.H. and Qin, Z.H. (2009) Strategies for short hairpin RNA delivery in cancer gene therapy. *Expert Opin Biol Ther*, **9**, 1357-1368.

46. Fellmann, C., Hoffmann, T., Sridhar, V., Hopfgartner, B., Muhar, M., Roth, M., Lai, D.Y., Barbosa, I.A., Kwon, J.S., Guan, Y. *et al.* (2013) An optimized microRNA backbone for effective single-copy RNAi. *Cell Rep*, **5**, 1704-1713.

47. Auyeung, V.C., Ulitsky, I., McGeary, S.E. and Bartel, D.P. (2013) Beyond secondary structure: primary-sequence determinants license pri-miRNA hairpins for processing. *Cell*, **152**, 844-858.

48. Kwan, K.M., Fujimoto, E., Grabher, C., Mangum, B.D., Hardy, M.E., Campbell, D.S., Parant, J.M., Yost, H.J., Kanki, J.P. and Chien, C.B. (2007) The Tol2kit: a multisite gateway-based construction kit for Tol2 transposon transgenesis constructs. *Dev. Dyn.*, **236**, 3088-3099.

49. Hoy, J.L., Constable, J.R., Vicini, S., Fu, Z. and Washbourne, P. (2009) SynCAM1 recruits NMDA receptors via protein 4.1B. *Mol. Cell. Neurosci.*, **42**, 466-483.

50. Barrow, S.L., Constable, J.R., Clark, E., El-Sabeawy, F., McAllister, A.K. and Washbourne, P. (2009) Neuroligin1: a cell adhesion molecule that recruits PSD-95 and NMDA receptors by distinct mechanisms during synaptogenesis. *Neural Dev*, **4**, 17.

51. Scheiffele, P., Fan, J., Choih, J., Fetter, R. and Serafini, T. (2000) Neuroligin expressed in nonneuronal cells triggers presynaptic development in contacting axons. *Cell*, **101**, 657-669.

52. Chih, B., Afridi, S.K., Clark, L. and Scheiffele, P. (2004) Disorder-associated mutations lead to functional inactivation of neuroligins. *Hum. Mol. Genet.*, **13**, 1471-1477.

53. Taniguchi, H., Gollan, L., Scholl, F.G., Mahadomrongkul, V., Dobler, E., Limthong, N., Peck, M., Aoki, C. and Scheiffele, P. (2007) Silencing of neuroligin function by postsynaptic neurexins. *J. Neurosci.*, **27**, 2815-2824.

54. Amarzguioui, M. and Prydz, H. (2004) An algorithm for selection of functional siRNA sequences. *Biochem. Biophys. Res. Commun.*, **316**, 1050-1058.

55. Fellmann, C., Zuber, J., McJunkin, K., Chang, K., Malone, C.D., Dickins, R.A., Xu, Q., Hengartner, M.O., Elledge, S.J., Hannon, G.J. *et al.* (2011) Functional identification of optimized RNAi triggers using a massively parallel sensor assay. *Mol. Cell*, **41**, 733-746.

56. Pei, Y. and Tuschl, T. (2006) On the art of identifying effective and specific siRNAs. *Nat. Methods*, **3**, 670-676.

57. Reynolds, A., Leake, D., Boese, Q., Scaringe, S., Marshall, W.S. and Khvorova, A. (2004) Rational siRNA design for RNA interference. *Nat. Biotechnol.*, **22**, 326-330.

58. Ui-Tei, K., Naito, Y., Takahashi, F., Haraguchi, T., Ohki-Hamazaki, H., Juni, A., Ueda, R. and Saigo, K. (2004) Guidelines for the selection of highly effective siRNA sequences for mammalian and chick RNA interference. *Nucleic Acids Res.*, **32**, 936-948.

59. Zuker, M. (2003) Mfold web server for nucleic acid folding and hybridization prediction. *Nucleic Acids Res.*, **31**, 3406-3415.

60. Darty, K., Denise, A. and Ponty, Y. (2009) VARNA: Interactive drawing and editing of the RNA secondary structure. *Bioinformatics*, **25**, 1974-1975.

61. Morgan, M., Anders, S., Lawrence, M., Aboyoun, P., Pages, H. and Gentleman, R. (2009) ShortRead: a bioconductor package for input, quality assessment and exploration of high-throughput sequence data. *Bioinformatics*, **25**, 2607-2608.

62. Dull, T., Zufferey, R., Kelly, M., Mandel, R.J., Nguyen, M., Trono, D. and Naldini, L. (1998) A third-generation lentivirus vector with a conditional packaging system. *J. Virol.*, **72**, 8463-8471.

63. Brewer, G.J., Torricelli, J.R., Evege, E.K. and Price, P.J. (1993) Optimized survival of hippocampal neurons in B27-supplemented Neurobasal, a new serum-free medium combination. *J. Neurosci. Res.*, **35**, 567-576.

64. Khvorova, A., Reynolds, A. and Jayasena, S.D. (2003) Functional siRNAs and miRNAs exhibit strand bias. *Cell*, **115**, 209-216.

65. Schwarz, D.S., Hutvagner, G., Du, T., Xu, Z., Aronin, N. and Zamore, P.D. (2003) Asymmetry in the assembly of the RNAi enzyme complex. *Cell*, **115**, 199-208.

66. Fogel, A.I., Akins, M.R., Krupp, A.J., Stagi, M., Stein, V. and Biederer, T. (2007) SynCAMs organize synapses through heterophilic adhesion. *J. Neurosci.*, **27**, 12516-12530.

67. Shabalina, S.A., Spiridonov, A.N. and Ogurtsov, A.Y. (2006) Computational models with thermodynamic and composition features improve siRNA design. *BMC Bioinformatics*, **7**, 65.

68. Jagla, B., Aulner, N., Kelly, P.D., Song, D., Volchuk, A., Zatorski, A., Shum, D., Mayer, T., De Angelis, D.A., Ouerfelli, O. *et al.* (2005) Sequence characteristics of functional siRNAs. *RNA*, **11**, 864-872.

69. Matveeva, O.V., Nazipova, N.N., Ogurtsov, A.Y. and Shabalina, S.A. (2012) Optimized models for design of efficient miR30-based shRNAs. *Front Genet*, **3**, 163.

70. Chalk, A.M., Wahlestedt, C. and Sonnhammer, E.L. (2004) Improved and automated prediction of effective siRNA. *Biochem. Biophys. Res. Commun.*, **319**, 264-274.

71. Betancur, J.G., Yoda, M. and Tomari, Y. (2012) miRNA-like duplexes as RNAi triggers with improved specificity. *Front Genet*, **3**, 127.

72. Yoda, M., Kawamata, T., Paroo, Z., Ye, X., Iwasaki, S., Liu, Q. and Tomari, Y. (2010) ATP-dependent human RISC assembly pathways. *Nat. Struct. Mol. Biol.*, **17**, 17-23.

73. Okamura, K., Liu, N. and Lai, E.C. (2009) Distinct mechanisms for microRNA strand selection by Drosophila Argonautes. *Mol. Cell*, **36**, 431-444.

74. Noland, C.L. and Doudna, J.A. (2013) Multiple sensors ensure guide strand selection in human RNAi pathways. *RNA*, **19**, 639-648.

75. Patzel, V., Rutz, S., Dietrich, I., Koberle, C., Scheffold, A. and Kaufmann, S.H. (2005) Design of siRNAs producing unstructured guide-RNAs results in improved RNA interference efficiency. *Nat. Biotechnol.*, **23**, 1440-1444.

76. Tomari, Y., Du, T. and Zamore, P.D. (2007) Sorting of Drosophila small silencing RNAs. *Cell*, **130**, 299-308.

77. Forstemann, K., Horwich, M.D., Wee, L., Tomari, Y. and Zamore, P.D. (2007) Drosophila microRNAs are sorted into functionally distinct argonaute complexes after production by dicer-1. *Cell*, **130**, 287-297.

78. Mori, M., Triboulet, R., Mohseni, M., Schlegelmilch, K., Shrestha, K., Camargo, F.D. and Gregory, R.I. (2014) Hippo signaling regulates microprocessor and links cell-density-dependent miRNA biogenesis to cancer. *Cell*, **156**, 893-906.

79. Moy, R.H., Cole, B.S., Yasunaga, A., Gold, B., Shankarling, G., Varble, A., Molleston, J.M., tenOever, B.R., Lynch, K.W. and Cherry, S. (2014) Stem-loop recognition by DDX17 facilitates miRNA processing and antiviral defense. *Cell*, **158**, 764-777.

80. Zhou, H., Xia, X.G. and Xu, Z. (2005) An RNA polymerase II construct synthesizes short-hairpin RNA with a quantitative indicator and mediates highly efficient RNAi. *Nucleic Acids Res.*, **33**, e62.

81. Osorio, L., Gijsbers, R., Oliveras-Salva, M., Michiels, A., Debyser, Z., Van den Haute, C. and Baekelandt, V. (2014) Viral vectors expressing a single microRNA-based short-hairpin RNA result in potent gene silencing in vitro and in vivo. *J. Biotechnol.*, **169**, 71-81.

82. Giacomotto, J., Rinkwitz, S. and Becker, T.S. (2015) Effective heritable gene knockdown in zebrafish using synthetic microRNAs. *Nat Commun*, **6**, 7378.

Chapter III

Benton, C.S., Miller, B.H., Skwerer, S., Suzuki, O., Schultz, L.E., Cameron, M.D., Marron, J.S., Pletcher, M.T., and Wiltshire, T. (2012). Evaluating genetic markers and neurobiochemical analytes for fluoxetine response using a panel of mouse inbred strains. Psychopharmacology (Berl) *221*, 297-315.

Biederer, T. (2006). Bioinformatic characterization of the SynCAM family of immunoglobulin-like domain-containing adhesion molecules. Genomics *87*, 139-150.

Biederer, T., Sara, Y., Mozhayeva, M., Atasoy, D., Liu, X., Kavalali, E.T., and Sudhof, T.C. (2002). SynCAM, a synaptic adhesion molecule that drives synapse assembly. Science *297*, 1525-1531.

Burton, S.D., Johnson, J.W., Zeringue, H.C., and Meriney, S.D. (2012). Distinct roles of neuroligin-1 and SynCAM1 in synapse formation and function in primary hippocampal neuronal cultures. Neuroscience *215*, 1-16.

Cheadle, L., and Biederer, T. (2012). The novel synaptogenic protein Farp1 links postsynaptic cytoskeletal dynamics and transsynaptic organization. J Cell Biol *199*, 985-1001.

Czondor, K., Garcia, M., Argento, A., Constals, A., Breillat, C., Tessier, B., and Thoumine, O. (2013). Micropatterned substrates coated with neuronal adhesion molecules for high-content study of synapse formation. Nat Commun *4*, 2252.

Dalva, M.B., McClelland, A.C., and Kayser, M.S. (2007). Cell adhesion molecules: signalling functions at the synapse. Nat Rev Neurosci *8*, 206-220.

Fogel, A.I., Akins, M.R., Krupp, A.J., Stagi, M., Stein, V., and Biederer, T. (2007). SynCAMs organize synapses through heterophilic adhesion. J Neurosci *27*, 12516-12530.

Fowler, D.K., Williams, C., Gerritsen, A.T., and Washbourne, P. (2015). Improved knockdown from artificial microRNAs in an enhanced miR-155 backbone: a designer's guide to potent multi-target RNAi. Nucleic Acids Res, doi: 10.1093/nar/gkv1246.

Garner, C.C., Zhai, R.G., Gundelfinger, E.D., and Ziv, N.E. (2002). Molecular mechanisms of CNS synaptogenesis. Trends Neurosci *25*, 243-251.

Gokce, O., and Sudhof, T.C. (2013). Membrane-tethered monomeric neurexin LNS-domain triggers synapse formation. J Neurosci *33*, 14617-14628.

Hoy, J.L., Constable, J.R., Vicini, S., Fu, Z., and Washbourne, P. (2009). SynCAM1 recruits NMDA receptors via protein 4.1B. Mol Cell Neurosci *42*, 466-483.

Kameda, H., Furuta, T., Matsuda, W., Ohira, K., Nakamura, K., Hioki, H., and Kaneko, T. (2008). Targeting green fluorescent protein to dendritic membrane in central neurons. Neurosci Res *61*, 79-91.

Kim, E., and Sheng, M. (2004). PDZ domain proteins of synapses. Nat Rev Neurosci *5*, 771-781.

Kim, J.H., Lee, S.R., Li, L.H., Park, H.J., Park, J.H., Lee, K.Y., Kim, M.K., Shin, B.A., and Choi, S.Y. (2011). High cleavage efficiency of a 2A peptide derived from porcine teschovirus-1 in human cell lines, zebrafish and mice. PLoS One *6*, e18556.

Kwan, K.M., Fujimoto, E., Grabher, C., Mangum, B.D., Hardy, M.E., Campbell, D.S., Parant, J.M., Yost, H.J., Kanki, J.P., and Chien, C.B. (2007). The Tol2kit: a multisite gateway-based construction kit for Tol2 transposon transgenesis constructs. Dev Dyn *236*, 3088-3099.

Levy, J.M., Chen, X., Reese, T.S., and Nicoll, R.A. (2015). Synaptic Consolidation Normalizes AMPAR Quantal Size following MAGUK Loss. Neuron *87*, 534-548.

Niculescu, A.B., Levey, D.F., Phalen, P.L., Le-Niculescu, H., Dainton, H.D., Jain, N., Belanger, E., James, A., George, S., Weber, H., *et al.* (2015). Understanding and predicting suicidality using a combined genomic and clinical risk assessment approach. Mol Psychiatry *20*, 1266-1285.

Redei, E.E., Andrus, B.M., Kwasny, M.J., Seok, J., Cai, X., Ho, J., and Mohr, D.C. (2014). Blood transcriptomic biomarkers in adult primary care patients with major depressive disorder undergoing cognitive behavioral therapy. Transl Psychiatry *4*, e442.

Robbins, E.M., Krupp, A.J., Perez de Arce, K., Ghosh, A.K., Fogel, A.I., Boucard, A., Sudhof, T.C., Stein, V., and Biederer, T. (2010). SynCAM 1 adhesion dynamically regulates synapse number and impacts plasticity and learning. Neuron *68*, 894-906.

Sandau, U.S., Alderman, Z., Corfas, G., Ojeda, S.R., and Raber, J. (2012). Astrocyte-specific disruption of SynCAM1 signaling results in ADHD-like behavioral manifestations. PLoS One *7*, e36424.

Sara, Y., Biederer, T., Atasoy, D., Chubykin, A., Mozhayeva, M.G., Sudhof, T.C., and Kavalali, E.T. (2005). Selective capability of SynCAM and neuroligin for functional synapse assembly. J Neurosci *25*, 260-270.

Schambach, A., Mueller, D., Galla, M., Verstegen, M.M., Wagemaker, G., Loew, R., Baum, C., and Bohne, J. (2006). Overcoming promoter competition in packaging cells improves production of self-inactivating retroviral vectors. Gene Ther *13*, 1524-1533.

Scheiffele, P. (2003). Cell-cell signaling during synapse formation in the CNS. Annu Rev Neurosci *26*, 485-508.

Shipman, S.L., Schnell, E., Hirai, T., Chen, B.S., Roche, K.W., and Nicoll, R.A. (2011). Functional dependence of neuroligin on a new non-PDZ intracellular domain. Nat Neurosci *14*, 718-726.

Shu, X., Lev-Ram, V., Deerinck, T.J., Qi, Y., Ramko, E.B., Davidson, M.W., Jin, Y., Ellisman, M.H., and Tsien, R.Y. (2011). A genetically encoded tag for correlated light and electron microscopy of intact cells, tissues, and organisms. PLoS Biol *9*, e1001041.

Stagi, M., Fogel, A.I., and Biederer, T. (2010). SynCAM 1 participates in axo-dendritic contact assembly and shapes neuronal growth cones. Proc Natl Acad Sci U S A *107*, 7568-7573.

Takayanagi, Y., Fujita, E., Yu, Z., Yamagata, T., Momoi, M.Y., Momoi, T., and Onaka, T. (2010). Impairment of social and emotional behaviors in Cadm1-knockout mice. Biochem Biophys Res Commun *396*, 703-708.

Tallafuss, A., Constable, J.R., and Washbourne, P. (2010). Organization of central synapses by adhesion molecules. Eur J Neurosci *32*, 198-206.

Thomas, L.A., Akins, M.R., and Biederer, T. (2008). Expression and adhesion profiles of SynCAM molecules indicate distinct neuronal functions. J Comp Neurol *510*, 47-67.

Um, J.W., Pramanik, G., Ko, J.S., Song, M.Y., Lee, D., Kim, H., Park, K.S., Sudhof, T.C., Tabuchi, K., and Ko, J. (2014). Calsyntenins function as synaptogenic adhesion molecules in concert with neurexins. Cell Rep *6*, 1096-1109.

Waites, C.L., Craig, A.M., and Garner, C.C. (2005). Mechanisms of vertebrate synaptogenesis. Annu Rev Neurosci *28*, 251-274.

Washbourne, P., Dityatev, A., Scheiffele, P., Biederer, T., Weiner, J.A., Christopherson, K.S., and El-Husseini, A. (2004). Cell adhesion molecules in synapse formation. J Neurosci *24*, 9244-9249.

Zhiling, Y., Fujita, E., Tanabe, Y., Yamagata, T., Momoi, T., and Momoi, M.Y. (2008). Mutations in the gene encoding CADM1 are associated with autism spectrum disorder. Biochem Biophys Res Commun *377*, 926-929.